

# NIRVAR: Network Informed Restricted Vector Autoregression

Brendan Martin<sup>1</sup>, Francesco Sanna Passino<sup>1</sup>, Mihai Cucuringu<sup>2,3,4</sup>, and Alessandra Luati<sup>1,5</sup>

<sup>1</sup>Department of Mathematics, Imperial College London, United Kingdom

<sup>2</sup>Department of Statistics, University of Oxford, United Kingdom

<sup>3</sup>Oxford-Man Institute of Quantitative Finance, University of Oxford, United Kingdom

<sup>4</sup>The Alan Turing Institute, London, United Kingdom

<sup>5</sup>Department of Statistical Sciences, University of Bologna, Italy

## Abstract

High-dimensional panels of time series often arise in finance and macroeconomics, where co-movements within groups of panel components occur. Extracting these groupings from the data provides a course-grained description of the complex system in question and can inform subsequent prediction tasks. We develop a novel methodology to model such a panel as a restricted vector autoregressive process, where the coefficient matrix is the weighted adjacency matrix of a stochastic block model. This network time series model, which we call the Network Informed Restricted Vector Autoregression (NIRVAR) model, yields a coefficient matrix that has a sparse block-diagonal structure. We propose an estimation procedure that embeds each panel component in a low-dimensional latent space and clusters the embedded points to recover the blocks of the coefficient matrix. Crucially, the method allows for network-based time series modelling when the underlying network is unobserved. We derive the bias, consistency and asymptotic normality of the NIRVAR estimator. Simulation studies suggest that the NIRVAR estimated embedded points are Gaussian distributed around the ground truth latent positions. On three applications to finance, macroeconomics, and transportation systems, NIRVAR outperforms competing models in terms of prediction and provides interpretable results regarding group recovery.

**Keywords** — random graphs, multivariate time series, spectral embedding, stochastic blockmodel.

## 1 Introduction

Panels of stochastic processes,  $\{(X_{1,t}, \dots, X_{N,t})'\}_{t \in \mathbb{Z}}$ , which exhibit co-movements between components are central to many scientific disciplines, including econometrics and macroeconomics. Often,  $X_{i,t}$  depends not only on its own past values, but also on the past values of a subset of other panel components,  $\{X_{j,s} : j \subseteq \{1, \dots, N\}, s < t\}$ . For large  $N$ , modelling via the time series vector autoregression (VAR) framework becomes prohibitive as the number of model parameters grows as  $O(N^2)$  and can quickly exceed the number of observations. Techniques from high-dimensional statistics that introduce some form of sparsity or dimensionality reduction are therefore required in this setting.

Many variants of the factor modelling approach of [Stock and Watson \(2002\)](#) where the large panel of time series are modelled as stemming from a relatively small number of common latent factors have been proposed in statistics and econometrics (see, for example, [Bai, 2003](#); [Fan et al., 2013](#)). Sparse regression methods using various regularised estimation procedures have also been proposed as a way to reduce the number of model parameters. Common methods are the Least Absolute Shrinkage and Selection Operator (LASSO; [Tibshirani, 1996](#)), Smoothly Clipped Absolute Deviation (SCAD; [Fan and Li, 2001](#)), and Least Angle Regression (LARS; [Efron et al., 2004](#)). Network time series approaches in which each univariate time series is observed on a vertex of a graph are also

---

Corresponding author: Brendan Martin – ✉ [b.martin22@imperial.ac.uk](mailto:b.martin22@imperial.ac.uk)

popular in the literature (see, for example [Dahlhaus, 2000](#); [Eichler, 2007](#); [Ahelegbey et al., 2016](#)). The graph can be observed or inferred from data, with the edges of the graph encoding the co-dependence structure of the multivariate time series. For example, [Zhu et al. \(2020\)](#) utilise an observed graph to model the multivariate time series. Often, each edge corresponds to a parameter in the time series model. Therefore, if the graph is sparse, the number of model parameters can be smaller than the number of observations, enabling estimation and then prediction. In the case that it is inferred from data, the graph itself is of interest for tasks such as clustering, link prediction, and estimation of the Granger causality relations between panel components ([Lancichinetti and Fortunato, 2009](#); [Zhang and Chen, 2018](#)).

This paper proposes a method for inferring a graph structure from multivariate time series data and using it to impose restrictions on the coefficient matrix of a VAR model. Since the network determines the restricted VAR, we call the model the Network Informed Restricted VAR (NIRVAR) model. There is an extensive literature on incorporating network effects into a VAR framework. [Zhu et al. \(2017\)](#) and [Knight et al. \(2016\)](#) independently propose a VAR model in which the network effect on a panel component is the average of its connected neighbours in an observed network. [Knight et al. \(2020\)](#) propose a Generalised Network Autoregressive (GNAR) model which allows for a time-varying observed network, and show the consistency of generalised least squares estimation of the model parameters. [Fan et al. \(2023\)](#) combine the dimensionality reduction of factor modelling with the parsimony of sparse linear regression and develop a hypothesis testing framework to determine the partial covariance structure. [Barigozzi et al. \(2023\)](#) extend this approach to the setting of dynamic factors, and propose an  $L_1$ -regularised Yule-Walker method for estimating a factor adjusted, idiosyncratic VAR model. The estimated VAR coefficients are then used for network estimation. [Chen et al. \(2023\)](#) introduce a network VAR model similar to that of [Zhu et al. \(2017\)](#) but allows for network effects between groups of panel components, assuming that the network adjacency matrix is observable and generated by a stochastic block model (SBM; [Holland et al., 1983](#)). [Guðmundsson and Brownlees \(2021\)](#) introduce a stochastic block VAR model in which the time series are partitioned into latent groups such that the spillover effects are determined by a SBM. A group detection algorithm is developed in which the VAR coefficients are estimated with the method of least squares and used to obtain an embedding on which  $K$ -means clustering can be applied.

The method we propose differs from existing works as it involves firstly detecting latent groups from a latent space representation of each time series, and secondly estimating the VAR coefficients. Carrying out estimation in this order is a key contribution of this paper. We avoid estimating a dense VAR parameter matrix as in [Guðmundsson and Brownlees \(2021\)](#) or specifying tuning and thresholding parameters as in [Barigozzi et al. \(2023\)](#). We also emphasise that, in contrast to [Zhu et al. \(2017\)](#), [Knight et al. \(2020\)](#), [Chen et al. \(2023\)](#) and [Barigozzi et al. \(2025\)](#), the NIRVAR estimator does not require the underlying network to be observable, which is a realistic setting in many real-world applications.

NIRVAR models a panel of multivariate time series as a VAR(1) in which the VAR coefficient matrix  $\Phi$  is the weighted adjacency matrix of some random graph,  $\mathcal{G} = (\mathcal{V}, \mathcal{E})$ , where each of the  $N$  vertexes in the node set  $\mathcal{V}$  has an associated  $d$ -dimensional latent position  $\theta_i \in \mathcal{H}$ ,  $i \in \mathcal{V}$ , with  $\mathcal{H} \subseteq \mathbb{R}^d$  being some latent space, and where  $\mathcal{E} \subseteq \mathcal{V} \times \mathcal{V}$  is a set of random edges. In particular, we model  $\mathcal{G}$  as a stochastic block model. Typically, in the random graphs literature, the latent positions are estimated through spectral embedding of the observed adjacency matrix. However, in the settings we consider, the realised graph and its adjacency matrix are unobserved. It is therefore necessary to construct latent positions directly from the observed time series rather than from an observed adjacency matrix. Once latent positions have been constructed, they are clustered into  $K$  communities and these communities are used to enforce zero constraints on the VAR coefficients. In particular, if the constructed latent positions of two panel components  $i$  and  $j$  belong to different clusters, then  $\Phi_{ij}$  is set to 0. In practice, the network implies a subset VAR model ([Lütkepohl, 2005](#)) whose unrestricted parameters will be estimated via least squares. The proposed estimation framework is based on spectral methods (see [Chen et al., 2021](#), for a recent overview). As such, we focus on a single lag VAR. There is a significant strand of literature that considers VAR models with higher-order lags; see [Nicholson et al. \(2020\)](#) and references therein.

The NIRVAR estimation procedure draws inspiration from the workflow rationalised in [Whiteley et al. \(2022\)](#): linear dimension reduction via principal component analysis, embedding, clustering, and graph construction. In particular, we compute the singular value decomposition (SVD) of concatenated sample covariance matrices, con-

sider the corresponding left singular vectors embedding, and cluster the embedded points via a Gaussian mixture model with  $K$  components. The embedding dimension is chosen as the number of eigenvalues of the sample covariance matrix that are larger than the upper bound of the support of the Marčenko-Pastur distribution (Marčenko and Pastur, 1967). A graph with  $K$  cliques is then constructed based on a binary allocation of each embedded point to its most probable Gaussian mixture component. The estimated communities are reconstructions of the blocks of the SBM. The NIRVAR estimator assumes that the probability  $p^{(\text{in})}$  of an edge forming within a block is 1, and the probability  $p^{(\text{out})}$  of an edge forming between blocks is 0. If  $p^{(\text{out})} > p^{(\text{in})}$ , the data generating SBM will have a large proportion of inter-block edges and the NIRVAR estimation framework will not capture any of these edges. We therefore restrict our attention to assortative SBMs (see Lee and Wilkinson, 2019, for a review of SBMs). Since the NIRVAR estimator does not recover edges between vertices in different blocks of the data generating SBM, the estimator will be biased whenever such inter-block edges are present. We derive the closed-form expression for the bias, prove consistency and asymptotic normality of the estimator, and discuss its asymptotic efficiency.

Each step of the NIRVAR estimation framework can be modified easily. For example, we also consider embedding via the SVD of the precision matrix. Although we do not pursue it here, one could imagine choosing the embedding dimension using, for example, the profile likelihood method of Zhu and Ghodsi (2006) or the ScreeNOT method of Donoho et al. (2023). The motivation for using a Gaussian mixture model instead of say,  $K$ -means clustering, is due to the literature on random dot product graphs (Rubin-Delanchy et al., 2022) which shows that spectral embedding yields uniformly consistent latent position estimates with asymptotically Gaussian error (up to identifiability).

NIRVAR can model data that is represented by a multiplex network, corresponding to a network containing multiple types of edges, expressed via a graph  $\mathcal{G}$  containing multiple layers of connectivity, one layer for each type of edge (De Domenico et al., 2013). If there are  $Q$  layers, or features, then the time series data we consider consists of  $NQ$  univariate series,  $\{X_{i,t}^{(q)}\}_{t \in \mathbb{Z}}$ , where  $q \in \{1, \dots, Q\}$ . These types of matrix time series have been considered by Chang et al. (2023), who propose a one-pass estimation procedure for a tensor canonical polyadic decomposition model of the matrix time series. Barigozzi et al. (2025) also employ a tensor-based principal component approach to a factor network autoregressive model. In contrast, to obtain latent embeddings in the case of multiple features, we unfold the tensor and compute the SVD of the concatenated sample covariance matrices across  $q$  features. This choice is motivated by the stability properties of the unfolded adjacency spectral embedding procedure discussed in Gallagher et al. (2021).

The rest of the paper is organised as follows. The NIRVAR model is defined in Section 2. Section 3 details our proposed estimation method and formally relates NIRVAR with the underlying weighted stochastic block model. Section 4 derives the finite and asymptotic properties of the NIRVAR estimator. The finite sample properties and the robustness of each stage of the estimation procedure are assessed through an extensive simulation study in Section 5. Section 6 illustrates the flexibility of NIRVAR across different tasks and in comparison with related network time series models through three applications to financial, macroeconomic and transportation data. The online supplementary material contains proofs and additional results from the empirical analyses. All data and code are available in the Github repository [bmartin9/NIRVAR](https://github.com/bmartin9/NIRVAR).

## 1.1 Notation

For an integer  $k$ , let  $[k]$  denote the set  $\{1, \dots, k\}$ . The  $n \times n$  identity matrix is written  $I_n$ , and the indicator function is  $\mathbb{1}\{\mathcal{B}\} = 1$  if the event  $\mathcal{B}$  occurs and 0 otherwise. For vectors,  $\mathbf{v}_1, \dots, \mathbf{v}_n \in \mathbb{R}^p$ , let  $M = (\mathbf{v}_1, \dots, \mathbf{v}_n) \in \mathbb{R}^{p \times n}$  be the matrix whose columns are given by  $\mathbf{v}_1, \dots, \mathbf{v}_n$ . The column space of  $M$  is  $\text{colsp}(M)$ , its rank is  $\text{rk}(M)$ , and its transpose is  $M'$ . We write  $M_{i,:}$  and  $M_{:,j}$  to denote the  $i$ -th row and  $j$ -th column of  $M$  considered as vectors, respectively. The element-wise  $\ell_0$  norm is defined as  $|M|_0 = \sum_{i=1}^p \sum_{j=1}^n \mathbb{1}\{M_{ij} \neq 0\}$ . The Frobenius norm is  $\|M\|_F = (\sum_{i=1}^p \sum_{j=1}^n |M_{ij}|^2)^{1/2}$ . The spectral radius of an  $n \times n$  matrix  $A$  is  $\rho(A) = \max\{|\lambda_1|, \dots, |\lambda_n|\}$  where  $\lambda_1, \dots, \lambda_n$  are the eigenvalues of  $A$ . The vectorisation operator  $\text{vec}(\cdot)$  transforms a  $p \times n$  matrix  $M$  into a  $pn \times 1$  vector by stacking its columns. Let  $\odot$  denote the Hadamard product between two matrices of the same dimensions, and  $\otimes$  denote the Kronecker product between two matrices, not necessarily of the same dimension. For matrices  $M_1, \dots, M_r$ , let  $(M_1 | \dots | M_r)$  and  $(M_1; \dots; M_r)$  denote the column-wise and row-wise concatenation of the

matrices, respectively. The set of  $n \times d$  matrices with orthogonal columns is  $\mathbb{O}(n \times d)$ . For a distribution  $F$  the support of  $F$  is  $\text{supp}(F)$ .

## 2 Model

Let  $(X_{i,t}^{(q)})$  be a matrix time series consisting of  $NQ$  random variables at each time  $t \in \mathbb{Z}$ . For example,  $i \in [N]$  could label an individual and  $q \in [Q]$  a particular variable or feature associated with that individual. Consider an associated multiplex network with  $Q$  layers each having  $N$  vertices. The random variable  $X_{i,t}^{(q)}$  is observed at vertex  $i$  of layer  $q$  of the multiplex network. For each feature  $q \in [Q]$  we associate a random graph  $\mathcal{G}^{(q)} = (\mathcal{V}, \mathcal{E}^{(q)})$  where  $\mathcal{V} = [N]$ .  $\mathcal{G}^{(q)}$  is modelled as a SBM. We utilise the random dot product graph (RDPG; Athreya et al., 2017) representation of the SBM since our subsequent estimation method involves constructing latent positions for each node, which are then clustered in order to recover the blocks of the SBM, providing a convenient mathematical framework.

**Definition 2.1** (Directed RDPG with distribution  $F$  and self-loops). *Let  $F$  be a  $d$ -dimensional distribution with support  $\text{supp}(F) = \mathcal{H} \subset \mathbb{R}^d$ , such that  $\mathbf{x}'\mathbf{y} \in [0, 1]$  for all  $\mathbf{x}, \mathbf{y} \in \mathcal{H}$ . Let  $\boldsymbol{\theta}_1, \dots, \boldsymbol{\theta}_N \sim F$  be the rows of the matrix  $\Theta = (\boldsymbol{\theta}_1, \dots, \boldsymbol{\theta}_N)' \in \mathbb{R}^{N \times d}$  and  $A$  a random adjacency matrix such that, conditional on  $\Theta$ :*

$$p(A | \Theta) = \prod_{i=1}^N \prod_{\substack{j=1 \\ j \neq i}}^N (\boldsymbol{\theta}'_i \boldsymbol{\theta}_j)^{A_{ij}} (1 - \boldsymbol{\theta}'_i \boldsymbol{\theta}_j)^{1-A_{ij}} \prod_{h=1}^N \mathbb{1}\{A_{hh} = 1\},$$

where  $p(\cdot)$  represents a probability mass function. Then we say that  $A$  is the adjacency matrix of a directed RDPG with self-loops of rank at most  $d$  and with latent positions given by the rows of  $\Theta$ , written  $(A, \Theta) \sim \text{RDPG}(F)$ .

**Remark 1.** *In contrast to the definition given by Athreya et al. (2017), Definition 2.1 does not restrict  $A$  to be symmetric and with principal diagonal elements equal to zero. This is to allow for directed graphs with self loops. With a slight abuse of notation, RDPG will be used in the rest of this work to denote a directed random dot product graph with self-loops.*

**Definition 2.2** ( $K$ -block SBM). *We say that  $(A, \Theta) \sim \text{RDPG}(F)$  is a SBM with  $K$  blocks or communities if the number of distinct rows in  $\Theta$  is  $K$ . We define the block membership function  $z : [N] \mapsto [K]$  such that  $z_i = z_j$  if and only if  $\boldsymbol{\theta}_i = \boldsymbol{\theta}_j$  (where  $z(i) \equiv z_i$ ). Under this representation,  $F(\boldsymbol{\theta}) = \sum_{k=1}^K \pi_k \delta(\boldsymbol{\theta} - \boldsymbol{\nu}_k)$ , where  $\boldsymbol{\nu}_k \in \mathbb{R}^d, k \in [K]$  are community-specific latent positions chosen such that  $\boldsymbol{\nu}'_k \boldsymbol{\nu}_\ell \in [0, 1]$  for all  $k, \ell \in [K]$ , and  $\boldsymbol{\pi} = (\pi_1, \dots, \pi_K)$  represent the prior probabilities of each node to belong to the  $k$ -th community, with  $\pi_k \geq 0$  for all  $k \in [K]$  and  $\sum_{k=1}^K \pi_k = 1$ . Here,  $\delta$  is the  $d$ -dimensional Dirac delta function. The between-community connection probabilities can be collected in a matrix  $B \in [0, 1]^{K \times K}$  with  $B_{k\ell} = \boldsymbol{\nu}'_k \boldsymbol{\nu}_\ell, \boldsymbol{\nu}_k, \boldsymbol{\nu}_\ell \in \mathbb{R}^d$  for  $k, \ell = 1, \dots, K$ , and we write  $(A, \Theta) \sim \text{SBM}(B, \boldsymbol{\pi})$ .*

Definition 2.2 only covers the case in which the matrix  $B \in [0, 1]^{K \times K}$  of between-block connection probabilities is positive semi-definite, corresponding to an assortative graph. The motivation for this assumption is to have a multivariate time series model in which there is greater co-movement between panel components within the same community than between communities. The generalised RDPG (Rubin-Delanchy et al., 2022) provides an extension to the indefinite case. We also assume that each feature-specific graph  $\mathcal{G}^{(q)} = (\mathcal{V}, \mathcal{E}^{(q)})$  with adjacency matrix  $A^{(q)}$  has an associated latent position matrix  $\Theta^{(q)}$  such that

$$(A^{(q)}, \Theta^{(q)}) \sim \text{SBM}(B^{(q)}, \boldsymbol{\pi}^{(q)}), \quad q = 1, \dots, Q,$$

where  $B^{(q)} \in [0, 1]^{K \times K}$  and  $\boldsymbol{\pi}^{(q)}$  are feature-specific SBM parameters. The probability of an edge forming between vertices  $i$  and  $j, i \neq j$ , is  $p_{ij}^{(q)} = B_{z_i z_j}^{(q)} = \boldsymbol{\theta}_i^{(q)'} \boldsymbol{\theta}_j^{(q)}$ , and the adjacency matrix corresponding to  $\mathcal{G}^{(q)}$  is

$$A_{ij}^{(q)} \sim \text{Bernoulli}\left(p_{ij}^{(q)}\right). \tag{1}$$

Given  $\mathcal{G}^{(q)}$ , we define the NIRVAR model as follows.

**Definition 2.3** (NIRVAR model). For some fixed  $q \in [Q]$ , let  $\{\mathbf{X}_t^{(q)}\}_{t \in \mathbb{Z}}$  denote a zero mean, second order stationary stochastic process where  $\mathbf{X}_t^{(q)} = (X_{1,t}^{(q)}, \dots, X_{N,t}^{(q)})' \in \mathbb{R}^N$  and  $q \in [Q]$ . The NIRVAR model for the  $q$ -th feature is

$$\mathbf{X}_t^{(q)} = \sum_{r=1}^Q (A_q^{(r)} \odot \tilde{\Phi}_q^{(r)}) \mathbf{X}_{t-1}^{(r)} + \boldsymbol{\epsilon}_t^{(q)}, \quad \boldsymbol{\epsilon}_t^{(q)} \sim \mathcal{N}(0, \Sigma), \quad (2)$$

in which the generic element of  $A_q^{(r)}$ ,  $r \in [Q]$  is given by Equation (1) and  $\tilde{\Phi}_q^{(r)}$ ,  $r \in [Q]$  is an  $N \times N$  matrix of fixed weights. The covariance matrix of the noise process,  $\Sigma$ , is assumed to be positive definite. Defining  $\Phi_q^{(r)} := A_q^{(r)} \odot \tilde{\Phi}_q^{(r)}$  and  $\Phi_q := (\Phi_q^{(1)} | \dots | \Phi_q^{(Q)})$ , we write  $\mathbf{X}_t^{(q)} \sim \text{NIRVAR}(\Phi_q)$ .

If, for each  $q \in [Q]$ ,  $\mathbf{X}_t^{(q)} \sim \text{NIRVAR}(\Phi_q)$ , then  $\mathbf{X}_t := (\mathbf{X}_t^{(1)'}, \dots, \mathbf{X}_t^{(Q)'})' \in \mathbb{R}^{NQ}$  is a VAR(1) process with coefficient matrix  $\Xi := (\Phi_1; \dots; \Phi_Q) \in \mathbb{R}^{NQ \times NQ}$ . Therefore,  $\mathbf{X}_t^{(q)}$  will be stable, and hence stationary, if  $\rho(\Xi) < 1$  (Lütkepohl, 2005).

**Remark 2.** In Definition 2.3, we define the NIRVAR model only for the  $q$ -th feature, which acts as the response or endogenous variable, whereas the features  $C_{-q} = [Q] \setminus \{q\}$  are interpreted as covariates or exogenous variables. Since we focus on the response of the  $q$ -th feature, we drop the subscript on  $A_q^{(r)}$ ,  $\tilde{\Phi}_q^{(r)}$ ,  $\Phi_q^{(r)}$ , and  $\Phi_q$  for the remainder of the paper.

It will be convenient when discussing estimation of the NIRVAR model to write Equation (2) in vectorised form. For this purpose, we recall  $\mathbf{X}_t := (\mathbf{X}_t^{(1)'}, \dots, \mathbf{X}_t^{(Q)'})'$  and define

$$Y^{(q)} := (\mathbf{X}_1^{(q)}, \dots, \mathbf{X}_T^{(q)}), \quad X := (\mathbf{X}_0, \dots, \mathbf{X}_{T-1}), \quad U^{(q)} := (\boldsymbol{\epsilon}_1^{(q)}, \dots, \boldsymbol{\epsilon}_T^{(q)}), \quad A := (A^{(1)} | \dots | A^{(Q)}).$$

We can then write Equation (2) for  $t = 1, \dots, T$  as  $Y^{(q)} = \Phi X + U^{(q)}$ , or, equivalently, as

$$\mathbf{y}^{(q)} = \text{vec}(\Phi X) + \text{vec}(U^{(q)}) = (X' \otimes I_N) \boldsymbol{\beta} + \mathbf{u}^{(q)}, \quad (3)$$

where  $\mathbf{y}^{(q)} := \text{vec}(Y^{(q)})$ ,  $\boldsymbol{\beta} := \text{vec}(\Phi)$ , and  $\mathbf{u}^{(q)} := \text{vec}(U^{(q)})$ . The number of non-zero elements of  $\boldsymbol{\beta}$  is given by  $M = |A|_0$ .

The model can be written in terms of an unrestricted  $M$ -dimensional vector  $\boldsymbol{\gamma}(A)$  whose elements belong to the set  $\{\beta_i : \text{vec}(A)_i \neq 0, i = 1, \dots, N^2Q\}$ . Additionally, an  $N^2Q \times M$  matrix  $R(A)$  is defined via the mapping  $R : \{0, 1\}^{N \times NQ} \rightarrow \{0, 1\}^{N^2Q \times M}$ , where

$$[R(A)]_{ij} := \text{vec}(A)_i \times \mathbb{1} \left\{ \sum_{k=1}^{i-1} \text{vec}(A)_k = j - 1 \right\}. \quad (4)$$

The constraints on  $\boldsymbol{\beta}$  can then be written as

$$\boldsymbol{\beta} = R(A) \boldsymbol{\gamma}(A). \quad (5)$$

Combining Equation (3) and Equation (5) finally yields

$$\mathbf{y}^{(q)} = (X' \otimes I_N) R(A) \boldsymbol{\gamma}(A) + \mathbf{u}^{(q)}.$$

### 3 Estimation

The NIRVAR estimation method proceeds by firstly imposing subset VAR restrictions through a binary matrix,  $\hat{A} \in \{0, 1\}^{N \times NQ}$ , and then estimating  $\boldsymbol{\gamma}(\hat{A})$ . To obtain  $\hat{A}$ , a low-dimensional latent representation of each panel component is found by embedding the sample covariance matrix in some latent space. Clustering the latent

positions then allows for the construction of a graph with adjacency matrix  $\hat{A}$ . The choice of the sample covariance matrix is motivated by the connection between the covariance matrix  $\Gamma$  and the VAR coefficient matrix  $\Phi$  proved in Proposition 3.1 below. Under the assumptions of the proposition,  $\Gamma$ , and in turn the sample covariance matrix, both inherit network properties of  $\Phi$  in terms of the underlying cluster structure.

The embedding and clustering method used here are in the spirit of Whiteley et al. (2022) who give theoretical justification for linear dimensionality reduction via principal component analysis, a subsequent embedding, and graph construction using the embedded points. The next sections describe how these steps are implemented in our setting.

### 3.1 Embedding

Let  $\mathcal{X}^{(q)} = (\mathbf{x}_1^{(q)}, \dots, \mathbf{x}_T^{(q)})$  be the  $N \times T$  design matrix of feature  $q$  where  $\mathbf{x}_t^{(q)} = (x_{1,t}^{(q)}, \dots, x_{N,t}^{(q)})'$  is a realisation of the random variable  $\mathbf{X}_t^{(q)}$ . To construct an embedding  $\hat{\psi}_i^{(q)} \in \mathbb{R}^d$  we are motivated by the unfolded adjacency spectral embedding (UASE, Jones and Rubin-Delanchy, 2020), which obtains embeddings  $\Psi^{(q)} \in \mathbb{R}^{N \times d}$  by considering the SVD of  $A = (A^{(1)} | \dots | A^{(Q)})$ . UASE has two key stability properties shown by Gallagher et al. (2021): it assigns the same position, up to noise, to vertices behaving similarly for a given feature (cross-sectional stability) and a constant position, up to noise, to a single vertex behaving similarly across different features (longitudinal stability). Since we do not observe  $A^{(q)}$ , we instead consider the SVD of  $S = (S^{(1)} | \dots | S^{(Q)}) \in \mathbb{R}^{N \times NQ}$  where  $S^{(q)} := \mathcal{X}^{(q)} \mathcal{X}^{(q)'} / T \in \mathbb{R}^{N \times N}$  is the sample covariance matrix for feature  $q$ . We can write  $S = UDV' + U_\perp D_\perp V_\perp'$ , where  $D \in \mathbb{R}^{d \times d}$  is a diagonal matrix containing the  $d$  largest singular values of  $S$ , and the columns of  $U \in \mathbb{O}(N \times d)$  and  $V \in \mathbb{O}(NQ \times d)$  are the corresponding  $d$  left and right singular vectors, respectively. Assuming  $S$  admits a low-rank approximation, UASE uses only  $\hat{S} = UDV'$  to produce embeddings. In particular, the  $q$ -th right UASE is the matrix  $\hat{\Psi}^{(q)} \in \mathbb{R}^{N \times d}$  obtained by dividing  $\hat{\Psi} = VD^{1/2} \in \mathbb{R}^{NQ \times d}$  into  $Q$  equal blocks,  $\hat{\Psi} = (\hat{\Psi}^{(1)}; \dots; \hat{\Psi}^{(Q)})$ . The feature- $q$  embedding of time series  $i$  is thus  $\hat{\psi}_i^{(q)} = (\hat{\Psi}^{(q)})_{i,:}$ .

It is of interest to relate  $\hat{\psi}_i^{(q)}$  to the ground truth latent positions  $\theta_i^{(q)}$ , since clustering of  $\hat{\psi}_i^{(q)}$  will be used to recover the blocks of the data generating SBM. We derive a connection between the covariance matrix  $\Gamma^{(q)} = \mathbb{E}\{(\mathbf{X}_t^{(q)})(\mathbf{X}_t^{(q)})'\}$  of a NIRVAR( $\Phi$ ) process and  $\theta_i^{(q)}$  for the case  $Q = 1$ . In the special case of symmetric  $\Phi$ , which is a standard assumption in the RDPG literature (see, for example Athreya et al., 2017), Proposition 3.1 shows that the rank  $d$  spectral embeddings of  $\Gamma^{(q)}$  and  $\Phi$  are equivalent. Since we assume  $Q = 1$  in Proposition 3.1, the superscript  $q$  is dropped for readability.

**Proposition 3.1.** *Let  $\mathbf{X}_t \sim \text{NIRVAR}(\Phi)$  and assume  $\Sigma = \sigma^2 I_N$ . If  $\Phi$  is symmetric with eigendecomposition  $\Phi = U_\Phi \Lambda_\Phi U_\Phi' + U_{\Phi,\perp} \Lambda_{\Phi,\perp} U_{\Phi,\perp}'$ , where  $U_\Phi \in \mathbb{O}(N \times d)$  and  $\Lambda_\Phi$  is a  $d \times d$  diagonal matrix comprising the  $d$  largest eigenvalues in absolute value of  $\Phi$ , then the rank  $d$  truncated eigendecomposition of the covariance matrix  $\Gamma = \mathbb{E}(\mathbf{X}_t \mathbf{X}_t')$  is  $\Gamma = U_\Gamma \Lambda_\Gamma U_\Gamma'$  in which  $\Lambda_\Gamma$  is a  $d \times d$  diagonal matrix with diagonal elements  $(\lambda_\Gamma)_i = 1/\{1 - (\lambda_\Phi)_i^2\}$  where  $(\lambda_\Phi)_i$  is the corresponding diagonal entry of  $\Lambda_\Phi$ .*

Under Proposition 3.1, the eigenvectors corresponding to the  $d$  largest eigenvalues of  $\Gamma$  and  $\Phi$  are the same. Therefore, the rank  $d$  spectral embedding of  $\Phi$  can be constructed, up to identifiability, from the eigenvectors and scaled eigenvalues of  $\Gamma$ , where the scaling is given by  $(\lambda_\Phi)_i = \pm \sqrt{1 - 1/(\lambda_\Gamma)_i}$ .

Gallagher et al. (2023) prove a central limit theorem for the asymptotic behaviour of  $\Psi_\Phi = U_\Phi \Lambda_\Phi^{1/2}$  where  $\Phi$  is an observed symmetric matrix sampled from a weighted RDPG. They prove that, up to a sequence of orthogonal transformations,  $(\Psi_\Phi)_i$  is asymptotically normally distributed around the ground truth latent positions,  $\theta_i$ . The relation between  $\Psi_\Gamma = U_\Gamma \Lambda_\Gamma^{1/2}$  and  $\Psi_\Phi$  shown by Proposition 3.1 suggests that there may be a similar connection between  $(\Psi_\Gamma)_i$  and  $\theta_i$ . A simulation study comparing  $(\Psi_\Gamma)_i$  and  $\theta_i$  is discussed in Section 5.

### 3.2 Clustering

Clustering via a Gaussian mixture model can be used to assign a label  $\hat{z}_i^{(q)} \in \{1, \dots, K\}$  to each panel component based on  $\hat{\psi}_i^{(q)}$ . In particular, we use Expectation-Maximisation to maximise the Gaussian mixture model incomplete log-likelihood and estimate the cluster assignments  $\hat{z}_i^{(q)}$ . We define  $\hat{A} = (\hat{A}^{(1)} | \dots | \hat{A}^{(Q)}) \in \{0, 1\}^{N \times NQ}$  as

$\hat{A}_{ij}^{(q)} = \mathbb{1}\{\hat{z}_j^{(q)} = \hat{z}_i^{(q)}\}$ . From this definition, it can be seen that  $\hat{A}$  defines a graph with  $K$  cliques and therefore cannot recover inter-block edges of the data generating SBM.

We use the following argument to motivate our choice of  $K$ . For a RDPG,  $A_{ij}^{(q)} \sim \text{Bernoulli}(\boldsymbol{\theta}_i^{(q)'} \boldsymbol{\theta}_j^{(q)})$  and thus  $\mathbb{E}(A^{(q)}) = \Theta^{(q)} \Theta^{(q)'}$ , where  $\Theta^{(q)} = (\boldsymbol{\theta}_1^{(q)}, \dots, \boldsymbol{\theta}_N^{(q)})' \in \mathbb{R}^{N \times d}$ . Assuming that  $\Theta^{(q)}$  is full rank, then  $\text{rank}\{\mathbb{E}(A^{(q)})\} = \text{rank}(\Theta^{(q)} \Theta^{(q)'}) = \text{rank}(\Theta^{(q)}) = d$ . For a SBM,  $\Theta^{(q)}$  has  $K$  distinct rows (corresponding to the  $K$  latent positions), and thus  $\text{rank}(\Theta^{(q)}) = K$ . Since we are assuming  $\mathcal{G}^{(q)}$  is a SBM, we set  $K = d$ .

### 3.3 Parameter estimation

The subset VAR restrictions we impose correspond to the zero entries of  $\hat{A}$ . Given  $\hat{A}$ , there are  $\widehat{M} = |\hat{A}|_0$  remaining unrestricted parameters that we estimate via least squares. Let  $\boldsymbol{\gamma}(\hat{A})$  be the  $\widehat{M}$ -dimensional vector of unrestricted parameters whose elements are those in the set  $\{\beta_i : \text{vec}(\hat{A})_i \neq 0, i = 1, \dots, N^2Q\}$ . Let  $R(\hat{A}) \in \{0, 1\}^{N^2Q \times \widehat{M}}$  be the restrictions matrix corresponding to  $\hat{A}$  where  $R$  is defined by Equation (4). The model corresponding to the estimated restrictions  $\hat{A}$  is

$$\mathbf{y}^{(q)} = (X' \otimes I_N) R(\hat{A}) \boldsymbol{\gamma}(\hat{A}) + \mathbf{u}(\hat{A})^{(q)}.$$

The least squares estimator of  $\boldsymbol{\gamma}(\hat{A})$  minimises the objective  $S\{\boldsymbol{\gamma}(\hat{A})\} = \mathbf{u}(\hat{A})^{(q)'} (I_T \otimes \Sigma^{-1}) \mathbf{u}(\hat{A})^{(q)}$ . Taking first derivatives and equating to zero yields the generalised least-squares estimator (GLS; see Section S1.2 of the supplementary material for the derivation)

$$\hat{\boldsymbol{\gamma}}(\hat{A}) = \{R(\hat{A})' (X X' \otimes \Sigma^{-1}) R(\hat{A})\}^{-1} R(\hat{A})' (X \otimes \Sigma^{-1}) \mathbf{y}^{(q)}. \quad (6)$$

Finally,

$$\hat{\boldsymbol{\beta}}(\hat{A}) = R(\hat{A}) \hat{\boldsymbol{\gamma}}(\hat{A}). \quad (7)$$

In the simulation studies in Section 5 and applications in Section 6, we assume that  $\Sigma = \sigma^2 I_N$ , implying that all the correlation among variables is explained by the network, in which case the GLS estimator (6) is the same as  $\hat{\boldsymbol{\gamma}}_{\text{OLS}}(\hat{A}) = \{R(\hat{A})' (X X' \otimes I_N) R(\hat{A})\}^{-1} R(\hat{A})' (X \otimes I_N) \mathbf{y}^{(q)}$ . The properties of these estimators are derived in Section 4.

### 3.4 Determining the embedding dimension

We employ tools from random matrix theory to estimate  $d^{(q)}$ , the rank of the RDPG  $\mathcal{G}^{(q)}$ . Following standard methods in the literature (see, for example, Laloux et al., 2000), our estimate  $\hat{d}^{(q)}$  is the number of eigenvalues of  $S^{(q)}$  that are larger than the upper bound of the support of the Marčenko-Pastur distribution (Marčenko and Pastur, 1967). The Marčenko-Pastur distribution is the limiting eigenvalue distribution of an  $N \times N$  Wishart matrix whose dimension to sample size ratio is a constant,  $\eta = N/T$ , and is given by

$$f_{\text{MP}}(x; \eta, \sigma^2) = \sqrt{(x - x_-)(x_+ - x)} / (2\pi\sigma^2\eta) \mathbb{1}\{x_- \leq x \leq x_+\},$$

with  $\sigma^2$  being the scale parameter and  $x_{\pm} = \sigma^2(1 \pm \sqrt{\eta})^2$  (for a derivation, see Bai and Silverstein, 2010). If  $\lambda_1^{(q)}, \dots, \lambda_N^{(q)}$  are the eigenvalues of  $S^{(q)}$ , then

$$\hat{d}^{(q)} = \sum_{j=1}^N \mathbb{1}\{\lambda_j^{(q)} > x_+\}.$$

The interpretation is that all eigenvalues that are greater than  $x_+$  cannot be attributed to random noise and are thus deemed as “informative”.

### 3.5 Alternative embeddings

Alternatives to the sample covariance matrix could be chosen for the embedding procedure described in Section 3.1. Here, we discuss embedding the precision matrix,  $\Omega^{(q)} = (S^{(q)})^{-1}$ . One motivation for the use of the precision matrix is its relation to the partial correlation  $\text{Cor}(Y_{i,:}^{(q)}, Y_{j,:}^{(q)} | Y_{-(i,j),:}^{(q)}) = \Omega_{ij}^{(q)} / (\Omega_{ii}^{(q)} \Omega_{jj}^{(q)})$ , where  $Y_{-(i,j),:}^{(q)}$  denotes the set of all rows of  $Y^{(q)}$  except rows  $i$  and  $j$ . We can thus interpret  $\Omega_{ij}^{(q)}$  as being proportional to the remaining correlation between time series  $i$  and time series  $j$  for feature  $q$  after the residual effect of all other time series has been removed. The unfolded adjacency spectral embedding and Gaussian mixture model clustering steps in the estimation procedure remain unchanged using the precision matrix. However, we need to slightly modify our method for estimating  $d^{(q)}$ . Instead of counting the number of eigenvalues of  $S^{(q)}$  that are larger than the upper bound of the support of the Marčenko-Pastur distribution, we count the number of eigenvalues of  $\Omega^{(q)}$  that are smaller than the lower bound of the support of the inverse Marčenko-Pastur distribution, which is the distribution of the reciprocal of a Marčenko-Pastur distributed random variable. The inverse Marčenko-Pastur distribution, derived in Section S1.6 of the supplementary material, is given by

$$f_{\text{IMP}}(y; \eta, \sigma^2) = (1 - \eta) \sqrt{(y_+ - y)(y - y_-)} / (2\pi\eta y^2) \mathbb{1}\{y_- \leq y \leq y_+\},$$

where  $y_{\pm} = \sigma^{-2} \{(1 - \eta)^{-1} (1 \pm \sqrt{\eta})\}^2$ . If  $\zeta_1^{(q)}, \dots, \zeta_N^{(q)}$  are the eigenvalues of  $\Omega^{(q)}$ , then our estimate of  $d^{(q)}$  when using the precision matrix becomes

$$\hat{d}^{(q)} = \sum_{j=1}^N \mathbb{1}\{\zeta_j^{(q)} < y_-\}.$$

## 4 Asymptotic properties

The GLS estimator given by Equation (7) is biased whenever an incorrect restriction is placed on the VAR matrix, that is, whenever  $\hat{A}_{ij}^{(q)} = 0$  but  $A_{ij}^{(q)} = 1$ , and unbiased otherwise. The following proposition establishes the conditions under which  $\hat{\beta}(\hat{A})$  is an unbiased estimator of  $\beta$  and specifies the bias whenever those conditions are not met.

**Proposition 4.1.** *Conditional on the estimated restrictions  $\hat{A}$ , the NIRVAR estimator  $\hat{\beta}(\hat{A})$  given by Equation (7) is unbiased if and only if  $\text{colsp}\{R(A)\} \subseteq \text{colsp}\{R(\hat{A})\}$ , where  $A$  specifies the true restrictions and  $\hat{A}$  specifies the estimated restrictions. When this condition is not satisfied,  $\mathbb{E}\{\hat{\beta}(\hat{A}) | \hat{A}\} = R(\hat{A})C\gamma(A)$ , where*

$$C := \{R(\hat{A})'(XX' \otimes \Sigma^{-1})R(\hat{A})\}^{-1}R(\hat{A})'(XX' \otimes \Sigma^{-1})R(A). \quad (8)$$

We now consider the asymptotic properties of  $\hat{\gamma}(\hat{A})$ .

**Proposition 4.2.** *The NIRVAR estimator  $\hat{\gamma}(\hat{A})$  given by Equation (6) is a consistent estimator of  $C\gamma(A)$  where  $C$  is defined by Equation (8), and*

$$\sqrt{T} \left\{ \hat{\gamma}(\hat{A}) - C\gamma(A) \right\} \xrightarrow{d} \mathcal{N} \left( 0, \left\{ R(\hat{A})' (\Gamma \otimes \Sigma^{-1}) R(\hat{A}) \right\}^{-1} \right),$$

where  $\Gamma := \mathbb{E}(X_t X_t') = \text{plim} XX' / T$ .

It is informative to compare the asymptotic efficiency of  $\hat{\gamma}(A)$  (the GLS estimator given that the true restrictions are known) with  $\hat{\gamma}(\hat{A})$  for the case where  $\text{colsp}\{R(A)\} \subseteq \text{colsp}\{R(\hat{A})\}$ , that is,  $\hat{A}$  contains no misspecified restriction, but may not include *all* of the true restrictions. The following proposition proves that, in this case,  $\hat{\gamma}(A)$  is asymptotically never less efficient than  $\hat{\gamma}(\hat{A})$ .

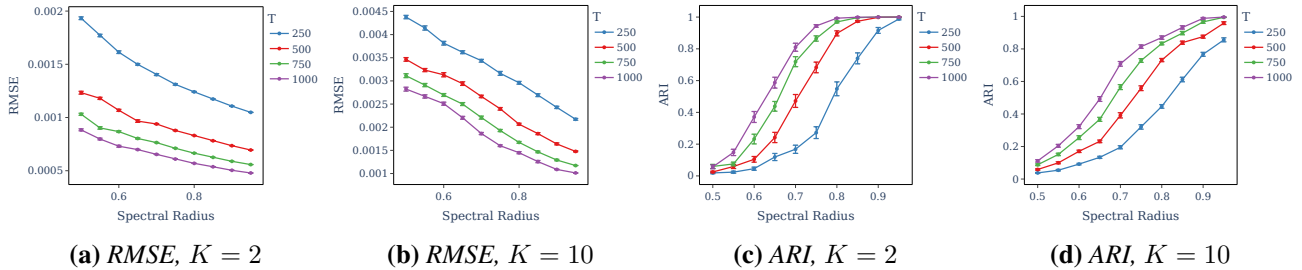


Figure 1: (a)-(b) Normalised RMSE of  $\hat{\Phi}$  and (c)-(d) ARI as  $\rho(\Phi)$  increases.

**Proposition 4.3.** Let  $\hat{\beta}(A) = R(A)\hat{\gamma}(A)$  and  $\hat{\beta}(\hat{A}) = R(\hat{A})\hat{\gamma}(\hat{A})$  be the GLS estimators given by Equation (7) for the case where  $A$  specifies the true restrictions of the data generating process and  $\hat{A}$  is another set of restrictions. Under the assumption that  $\text{colsp}\{R(A)\} \subseteq \text{colsp}\{R(\hat{A})\}$ , the asymptotic variance of  $\hat{\beta}(\hat{A})$  is greater than or equal to that of  $\hat{\beta}(A)$  in the sense that

$$\text{var} \left[ \sqrt{T} \left\{ \hat{\beta}(\hat{A}) - \beta \right\} \right] - \text{var} \left[ \sqrt{T} \left\{ \hat{\beta}(A) - \beta \right\} \right] \succeq 0,$$

where  $\succeq$  denotes positive semi-definite.

The extent to which the asymptotic variance of  $\hat{\gamma}(\hat{A})$  is inflated is discussed in Section 5.

## 5 Simulation study

We conduct an extensive simulation study with four main objectives. We simulate the underlying network from a stochastic block model with  $B_{kh} = p^{(\text{in})} \in [0, 1]$  for  $k = h$  and  $B_{kh} = p^{(\text{out})} \in [0, 1]$  for  $k \neq h$ ,  $k, h \in [K]$ . Firstly, we check whether NIRVAR cluster recovery and parameter estimates improve as the spectral radius of the ground truth VAR coefficient matrix  $\rho(\Phi)$  increases. We expect this to be the case since  $\rho(\Phi)$  controls the signal-to-noise ratio of the data generating process. Secondly, the ability of the NIRVAR estimator to obtain the correct restrictions should decrease as the number of edges between blocks increases. We thus count the number of errors in  $\hat{A}$  as a function of the probability  $p^{(\text{out})}$  of an edge forming between blocks in the simulated data generating process. Thirdly, the distribution of parameter estimates  $\hat{\gamma}(\hat{A})$  obtained from a large finite sample is compared with the asymptotic one in Proposition 4.2 and the asymptotic variance inflation given in Proposition 4.3 is quantified. Lastly, we compare the NIRVAR estimated latent positions with the ground truth latent positions of the data generating SBM. A further study showing the stability properties of UASE on the sample covariance matrix is reported in Section S2.2 of the supplementary material.

### 5.1 Spectral radius

The hyperparameters used to generate data from the NIRVAR model were  $N = 100$ ,  $Q = 1$ ,  $K \in \{2, 10\}$ , and  $T \in \{250, 500, 750, 1000\}$ . To set  $\tilde{\Phi}$ , we sampled each entry  $\tilde{\Phi}_{ij}$  independently from a Uniform(0,1) distribution and then normalised such that  $\rho(\Phi) \in \{0.5, 0.55, 0.6, 0.65, 0.7, 0.75, 0.8, 0.85, 0.9, 0.95\}$ . For each combination of  $\rho(\Phi)$  and  $T$ , we sampled  $\mathbf{X}_t^{(q)} \sim \text{NIRVAR}(\Phi)$ , obtained an estimate  $\hat{\Phi}$  of  $\Phi$  from the simulated data, and computed the normalised root mean squared error  $\text{NRMSE} = \|\hat{\Phi} - \Phi\|_F / (\hat{M}\rho(\Phi))$  and the Adjusted Rand Index (ARI, Hubert and Arabie, 1985), a measure of similarity between two clusterings of data. ARI ranges from -1 to 1, with higher values indicating stronger similarity. Averages over 15 replications are obtained, with the corresponding standard errors. Figure 1 (a) and (b) show that the NRMSE decreases both as  $\rho(\Phi)$  increases and as  $T$  increases. Figure 1 (c) and (d) show that the ARI approaches 1 as the spectral radius approaches 1, meaning that the true clusters are recovered in a high signal-to-noise regime.

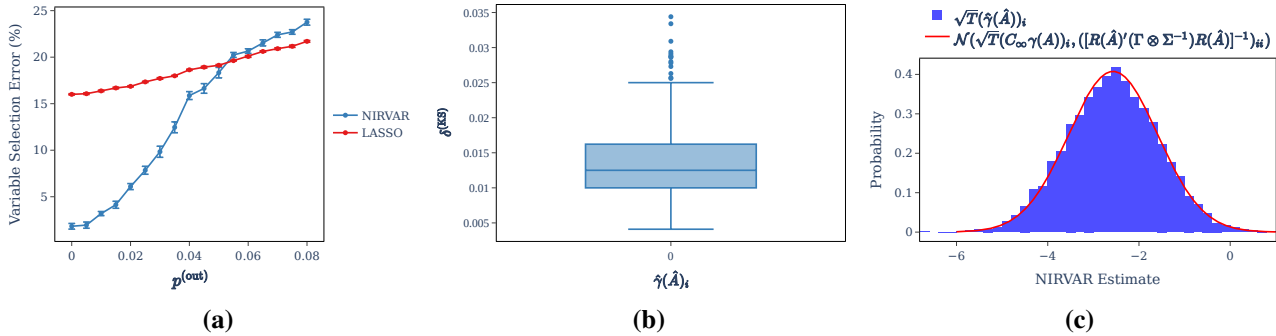


**Figure 2:** (a) Percentage error in estimated restrictions as  $p^{(out)}$  increases. (b) KS statistic: empirical and asymptotic distribution of  $\hat{\gamma}(\hat{A})_i$ , for  $i = 1, \dots, \hat{M}$ . (c) Histogram of  $\hat{\gamma}(\hat{A})_i$  for one fixed  $i$  and asymptotic distribution.

## 5.2 Between block probability

Fixing  $N = 100$ ,  $T = 1000$ ,  $Q = 1$ ,  $K = 10$ , and setting  $\tilde{\Phi}^{(1)}$  by sampling each entry from a Uniform(0,1) and normalising so that  $\rho(\Phi^{(1)}) = 0.9$ , we computed the percentage of incorrect entries of  $\hat{A}$  as a function of  $p^{(out)}$ . The percentage error was calculated as  $100 \times \sum_{i,j=1}^N \mathbb{1}\{\hat{A}_{ij} \neq A_{ij}\} / N^2$  and compared to the percentage variable selection error of a LASSO estimator, with penalty chosen using AIC. Figure 2(a) shows that for  $p^{(out)} < 0.05$  NIRVAR outperforms the LASSO. The percentage error increases with  $p^{(out)}$  and becomes larger than, though on the same scale as, that of the LASSO estimator for  $p^{(out)} > 0.05$ . This is expected since the NIRVAR estimation procedure always constructs a graph with  $K$  cliques and cannot recover edges between blocks.

## 5.3 Large sample distribution of the NIRVAR estimator

We simulate data with  $N = 50$ ,  $Q = 1$ ,  $T = 5000$ ,  $K = 5$ , and set  $\tilde{\Phi}^{(1)}$  by sampling each entry from a Uniform(0,1) and normalising so that  $\rho(\Phi^{(1)}) = 0.9$ . The probability of an edge forming within each block was set to  $p^{(in)} = 0.75$  and we set  $p^{(out)} = 0.2$ . Creating 10,000 replica datasets, each having these hyperparameters, and estimating  $\Phi$  for each replica provides an empirical distribution for  $\sqrt{T}\hat{\gamma}(\hat{A})_i$ . For each  $i = 1, \dots, \hat{M}$ , we performed a one-sample Kolmogorov-Smirnov (KS) test of whether the empirical distribution of  $\sqrt{T}\hat{\gamma}(\hat{A})_i$  is normal with mean  $\sqrt{T}C_\infty\gamma(A)$  and variance  $\{R(\hat{A})'(\Gamma \otimes \Sigma^{-1})R(\hat{A})\}^{-1}$  as claimed by Proposition 4.2 to be its asymptotic distribution, where  $C_\infty := \text{plim}(C) = \{R(\hat{A})'(\Gamma \otimes \Sigma^{-1})R(\hat{A})\}^{-1}R(\hat{A})'(\Gamma \otimes \Sigma^{-1})R(A)$ . Figure 2(b) shows a box plot of the KS statistic for each  $i = 1, \dots, \hat{M}$ , whilst Figure 2(c) shows a histogram of the observed sample for one particular  $i$  plotted alongside the corresponding asymptotic normal curve. The low value of  $\delta^{(KS)}$  shown by the box plot in Figure 2(b) indicates that the large sample distribution of  $\sqrt{T}\hat{\gamma}(\hat{A})_i$  mirrors the asymptotic distribution of Proposition 4.2. Under the same simulation setting, the asymptotic variance of the NIRVAR estimator is compared with an estimator that uses all ground truth restrictions where the intra-block sparsity of the ground truth is 50%. Defining  $\alpha_V := \text{tr}[\text{var}\{\hat{\beta}(\hat{A})\}] / \text{tr}[\text{var}\{\hat{\beta}(A)\}]$  as a measure of the extent to which the asymptotic variance of the NIRVAR estimator is inflated yields a value of  $\alpha_V = 1.8$ . The variation of  $\alpha_V$  with different levels of sparsity and different values of  $N$  is investigated (on synthetic and real data) in Section S2.1 of the supplementary material.

## 5.4 Latent position recovery

We conduct a study in which we fix two ground truth latent positions  $\theta_{B1} = (0.05, 0.95)'$  and  $\theta_{B2} = (0.95, 0.05)'$  of the data generating SBM and compare the (rotated) NIRVAR embedded points  $\hat{\Psi}^{(1)}$  to  $\theta_{B1}$  and  $\theta_{B2}$ . The hyperparameters used to generate the data were  $N = 150$ ,  $T = 2000$ ,  $Q = 1$ ,  $K = 2$ ,  $z_1, \dots, z_{75} = 1$  and  $z_{76}, \dots, z_{150} = 2$ . The weights  $\tilde{\Phi}$  were set to the constant  $0.9/\rho(\Theta\Theta')$  so that the spectral radius of the expected value of  $\Phi$  was 0.9. With  $\mathbf{X}_t^{(1)} \sim \text{NIRVAR}(\Phi)$  for  $t = 1, \dots, T$ , the left singular vectors and singular values of  $S^{(1)}$  were computed, and the singular values were scaled using  $(\lambda_\Phi)_i = \pm\sqrt{1 - 1/(\lambda_\Gamma)_i}$  from Proposition

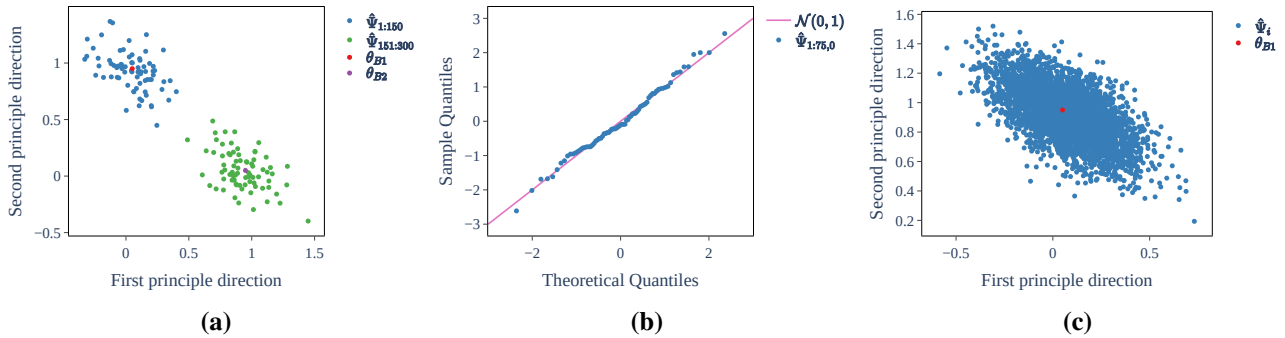


**Figure 3:** (a) NIRVAR embedded latent points (scaled and rotated) and true latent positions from the simulated SBM. (b) Q-Q plot comparing the sample distribution of the NIRVAR embedded points with a normal distribution. (c) The NIRVAR embedded latent position for  $i = 21$  across 4000 replica samples.

3.1. Procrustes alignment (Schönemann, 1966) was then used to compare the rotated sample embedded points  $\hat{\Psi}_{1:75}$  to  $\theta_{B1}$  and  $\hat{\Psi}_{76:150}$  to  $\theta_{B2}$ . Figure 3(a) shows  $\hat{\Psi}_i$  coloured according to the block membership  $z_i$  for  $i = 1, \dots, N$ . Figure 3(b) shows a Q-Q plot comparing the (standardised) sample distribution  $\hat{\Psi}_{1:75}$  with a standard normal distribution. The sample data is in good agreement with a normal distribution. We also conduct a further experiment in which we replicate the above procedure 4000 times and plot  $\hat{\Psi}_i$  for  $i = 21$  against  $\theta_{B1}$  across the 4000 replicas. Since  $\rho(\Phi_k)$  (with  $k \in \{1, \dots, 4000\}$  labelling the replica) has spectral radius less than 1 only in expectation, we only retain the first 4000 samples that have  $\rho(\Phi_k) < 1$ . Figure 3(c) shows that the large sample distribution of  $\hat{\Psi}_{21}$  is approximately normally distributed around  $\theta_{B1}$ . With the R package MVN (Korkmaz et al., 2014), we performed the Henze-Zirkler test of multivariate normality on the 4000 sample points yielding a test statistic of 0.56 and an observed  $p$ -value of 0.96 which supports the null hypothesis that the data is multivariate normally distributed.

## 6 Applications

The NIRVAR model is applied to three data sets exhibiting different characteristics: (i) a financial dataset of excess market returns, where multiplex NIRVAR can be applied based on different embeddings, allowing us to compare several model specifications; (ii) a vintage of macro-economic indicators typically used for predicting US industrial production; (iii) a transportation dataset of bicycle rides in London, where underlying groups are neither pre-determined nor necessarily related to geographical coordinates, and their flows and directions are of interest. Details of each dataset are reported in the following subsections.

To position NIRVAR within the most recent literature on network models for dynamic processes, results are compared with those from three related models, namely the Factor Augmented Regression Model (FARM) of Fan et al. (2023), the Factor-Adjusted Network Estimation and Forecasting for High-Dimensional Time Series (FNETS) model of Barigozzi et al. (2023), and the Generalised Network Autoregressive Processes (GNAR) model of Knight et al. (2020), whose specifications are reported in the supplementary materials.

### 6.1 Financial application to US equity market

The open-to-close (OPCL) and previous close-to-close (pvCLCL) price returns of  $N = 648$  financial assets between 03/01/2000 and 31/12/2020 ( $T = 5279$ ) were derived from databases provided by the Center for Research in Security Prices, LLC, an affiliate of the University of Chicago Booth School of Business. Using the S&P 500 index as a proxy for the market, we construct the OPCL and pvCLCL market excess returns by subtracting the return of SPY, the exchange traded fund which tracks the S&P 500 index. The task is to predict the next day pvCLCL market excess returns. If the predicted next day pvCLCL market excess return of an asset has a positive (negative) sign, then a long (short) position in the asset is taken. We compare seven different models: NIRVAR

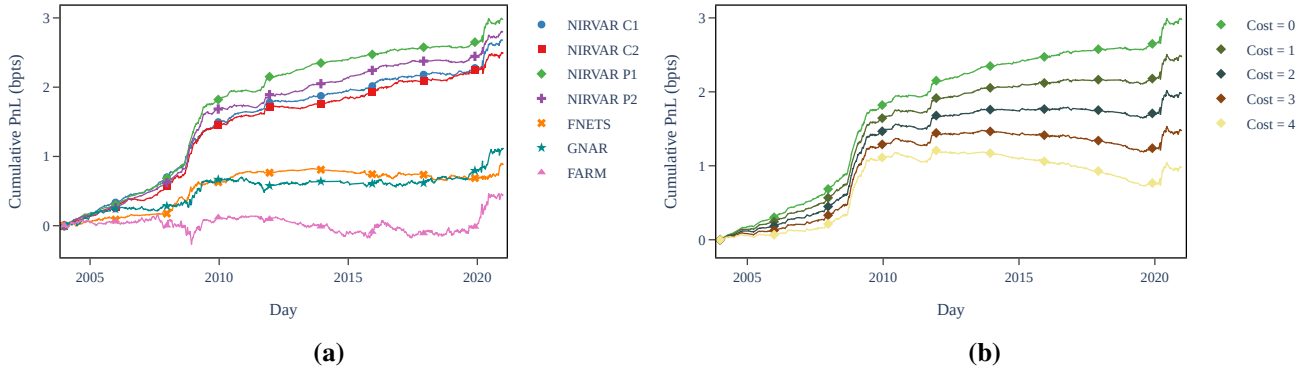


**Figure 4:** (a) Cumulative PnL in bpts for the 7 models with zero transaction costs. (b) Cumulative PnL of NIRVAR P1 for different levels of transaction costs.

using the covariance matrix embedding method with  $Q = 1$  (pvCLCL returns only) and  $Q = 2$  (pvCLCL and OPCL), labelled as NIRVAR C1 and NIRVAR C2, respectively; NIRVAR using the precision matrix embedding method with  $Q = 1$  and  $Q = 2$ , labelled as NIRVAR P1 and NIRVAR P2, respectively; FARM with  $L = 1$ ; FNETS with  $L = 1$ ; GNAR with  $L = 1$  and network  $\mathcal{G} = ([N], \mathcal{E})$  where  $(i, j) \in \mathcal{E}$  if asset  $i$  and asset  $j$  share the same Standard Industrial Classification (SIC) division. The SIC is a four-digit code assigned to businesses according to their industry, each belonging to one the following sectors: (i) Agriculture, Forestry, and Fishing, (ii) Mining, (iii) Construction, (iv) Manufacturing, (v) Transportation and Public Utilities, (vi) Wholesale Trade, (vii) Retail Trade, (viii) Finance, Insurance, and Real Estate, (ix) Services, and (x) Public Administration.

We backtest each model using a rolling window between 01/01/2004 and 31/12/2020 with a look-back window of four years and evaluate the performance via a number of commonly used metrics in the financial literature (see, for example Gu et al., 2020). Each day, we compute a measure of profit and loss,  $\text{PnL}_t = \sum_{i=1}^N \text{sign}(\hat{s}_i^{(t)}) \times s_i^{(t)}$ , where  $\hat{s}_i^{(t)}$  is the predicted return of asset  $i$  on day  $t$ , and  $s_i^{(t)}$  is the realised return of asset  $i$  on day  $t$ . Note that we assign an equal portfolio weighting to each asset in our definition of  $\text{PnL}_t$ ; an alternative approach would be to consider value-weighted portfolio construction methods, that account for the liquidity of each asset. The cumulative PnL for each model is shown in Figure 4(a). All NIRVAR models outperform FNETS, GNAR and FARM in terms of cumulative PnL, and NIRVAR P1 attains the highest cumulative PnL overall. We plot the cumulative PnL of NIRVAR P1 for different levels of transaction costs in Figure 4(b), where a flat transaction cost (given in basis points, denoted *bpts*, with 1% = 100bpts) is applied every time we flip our position in a given asset from long (short) to short (long). From Figure 4(b) we conclude that, even with a transaction cost of 4bpts, NIRVAR is profitable, especially during the global financial crisis and the COVID-19 pandemic which were periods of high market volatility. Table 1 reports the Mean Absolute Error (MAE) for all the estimated models, and the annualised Sharpe Ratio (SR) over 252 trading days. The SR is one of the most commonly used metrics in the financial industry, defined as  $\text{SR} = \sqrt{252} \times \text{mean}(\text{PnL}) / \text{stdev}(\text{PnL})$ . Although the MAE is equivalent across models, the SR is much larger for NIRVAR models, seemingly due to the best performance during crises. Buying and holding SPY across the same time period would yield a SR of 0.43, highlighting that NIRVAR models can provide greater economic benefits compared with a simple passive investment strategy. Within a financial context, MAE and other related metrics are not as representative as in traditional time series settings: since the profit or loss of a trade is assessed exclusively on whether it is a buy or a sell, different methods can attain significantly different Sharpe Ratios, despite having similar MAE (see, for example Vuletić et al., 2024). Further measures, reported in Tables S.1 and S.2 in the supplementary material, confirm that NP1 or NP2 consistently outperform the competing models.

Figure 5(a) compares the NIRVAR estimated clusters with the 10 SIC sectors on one particular backtesting day. Figure 5(b) shows the corresponding ARI for every backtesting day. The ARI never breaches 0.17, from which we conclude that the NIRVAR estimated clusters do not agree with SIC groupings. The bar chart does suggest, however, that NIRVAR tends to separate Finance, Insurance, and Real Estate companies from the other SIC groups.

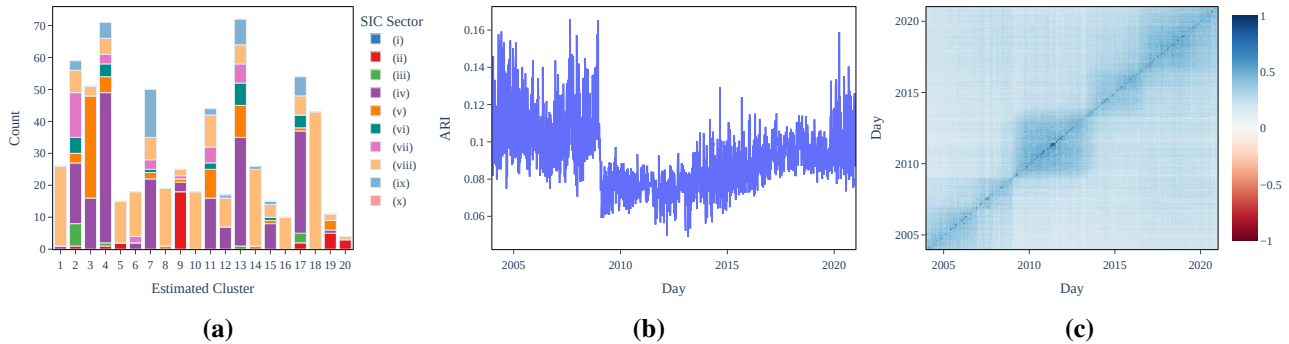


**Figure 5:** (a) Comparison of the NIRVAR estimated clusters with the SIC groups on 31/12/2020. (b) The ARI between the NIRVAR estimated clusters and the SIC groups on each backtesting day. (c) The ARI between NIRVAR estimated clusters on different days.

	N C1	N C2	N P1	N P2	FARM	FNETS	GNAR
Sharpe Ratio	2.50	2.34	2.82	2.69	0.22	0.78	0.70
Mean Absolute Error	0.012	0.013	0.012	0.013	0.012	0.012	0.012

**Table 1:** Sharpe Ratio and Mean Absolute Error values for the estimated models.

Figure 5(c) provides the ARI between the NIRVAR estimated clusters at time  $t$  and the NIRVAR estimated clusters at time  $s$ , where  $t$  and  $s$  run over every pair of backtesting days. There are two distinct blocks along the diagonal of this heatmap, the first one between 2004-2008 and the second one between 2008-2013, indicating that the NIRVAR estimated clusters underwent a shift after the global financial crisis.

## 6.2 US Industrial Production

FRED-MD<sup>1</sup> (McCracken and Ng, 2016) is a publicly accessible database of monthly observations of macroeconomic variables, updated in real-time. To allow direct comparison with Fan et al. (2023), we choose the August 2022 vintage of the FRED-MD database which extends from January 1960 until December 2019 ( $T = 719$ ), preprocessed as discussed in McCracken and Ng (2016). Only variables with no missing values ( $N = 122$ ) are used.

The task is one-step ahead prediction of the first-order difference of the logarithm of the monthly industrial production (IP) index. We backtest each model from January 2000 until December 2019 using a rolling window with a look-back window of 480 observations. The covariance matrix embedding method of NIRVAR is chosen. Following Fan et al. (2023), we set  $L = 24$  for FARM. For FNETS and GNAR we set  $L = 1$ . The FRED-MD variables are divided into eight groups: (i) output and income; (ii) labour market; (iii) housing; (iv) consumption, orders, and inventories; (v) money and credit; (vi) interest and exchange rates; (vii) prices; and (viii) stock market. The network  $\mathcal{G} = ([N], \mathcal{E})$  chosen for GNAR is defined by  $(i, j) \in \mathcal{E}$  if and only if  $i$  and  $j$  are in the same FRED-MD group.

The overall MSE of the NIRVAR estimator (0.0087) is smaller than the MSE of FARM (0.0089), which is the benchmark in this example, of FNETS (0.0096) and of GNAR (0.0101), that is based on an imposed network that coincides with the FRED-MD groups. NIRVAR estimation and prediction is also implemented using the imposed network that coincides with the FRED-MD groups, yielding an overall MSE of 0.0097. This highlights the utility of a data driven approach to group selection and network construction. As in Fan et al. (2023), we compute the ratio of cumulative MSEs between NIRVAR and each of FNETS, GNAR, and FARM. Letting  $\Delta_t^{(m)}$  be the ratio for model  $m \in \{\text{FNETS, GNAR, FARM}\}$  at time  $t \in \{1, \dots, T\}$ , we have  $\Delta_t^{(m)} := \sum_{s=1}^t \text{MSE}_s^{(\text{NIRVAR})} /$

<sup>1</sup>The database is available at <https://research.stlouisfed.org/econ/mccracken/fred-databases>.

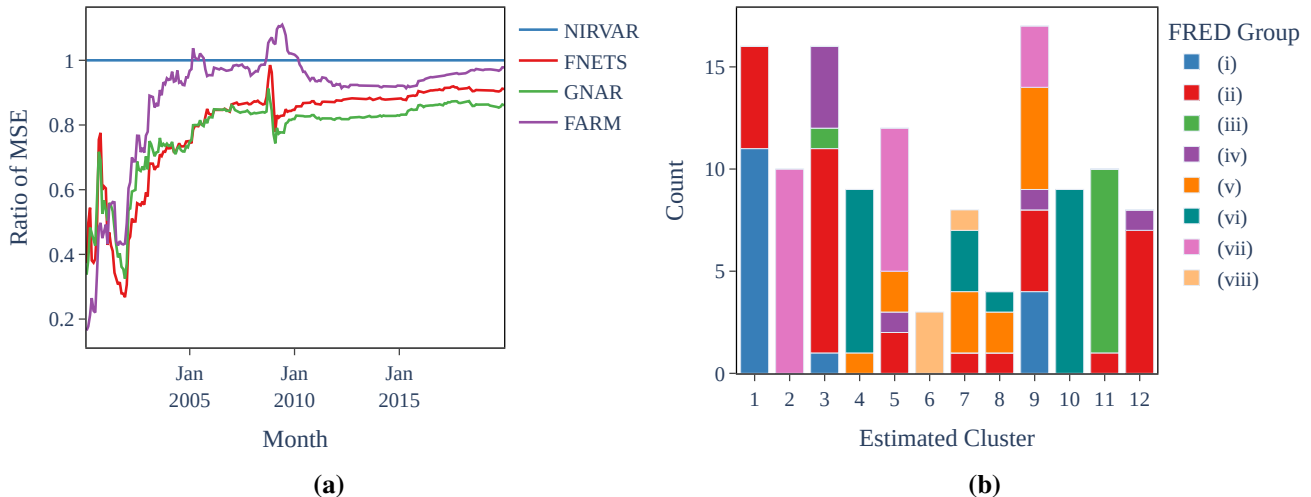


**Figure 6:** (a) Ratio  $\Delta_t^{(m)}$  of the cumulative MSE of NIRVAR divided by the cumulative MSE of alternative models. (b) Comparison of the NIRVAR estimated clusters with the FRED groups for January 2000.

$\sum_{s=1}^t \text{MSE}_s^{(m)}$ . A value of  $\Delta_t^{(m)}$  that is less than 1 indicates that NIRVAR is outperforming model  $m$  in terms of cumulative MSE. Figure 6(a) evidences that  $\Delta_t^{(m)}$  is always below 1 for GNAR and FNETS, and, for FARM, it is below 1 the majority of the time.

Figure 6(b) compares the  $K = 12$  NIRVAR estimated clusters with the eight FRED-MD groups on the first month of backtesting. NIRVAR clusters do not match the FRED-MD groups closely (the ARI for each backtesting time is in the range  $[0.24, 0.36]$ ). However, NIRVAR clusters 2, 4, 10, 11, and 12 are in close correspondence with individual FRED-MD groups, while NIRVAR cluster 1 largely recovers FRED-MD groups (i)-(ii), that are output and income and labour market. Clusters 3, 5, 7, 8, and 9 tend to aggregate FRED-MD financial sectors (v)-(viii). This is in line with the property of NIRVAR to model time series in which there is greater co-movement within communities than between communities.

The sensitivity of the estimators to extreme regimes is further explored in the supplementary materials, where we conclude that in this example, FNETS produces accurate predictions in non-crisis times while NIRVAR outperforms the competing models during crises, which is consistent with the results obtained in Section 6.1.

### 6.3 Santander bicycle rides

The first differences of the log daily number of bicycle rides from  $N = 774$  Santander stations in London from 07/03/2018 until 10/03/2020 ( $T = 735$ ) were obtained using records from TfL Open Data (see <https://cycling.data.tfl.gov.uk/>). Since  $N > T$ , the covariance matrix is not invertible and therefore the NIRVAR precision matrix embedding method is not feasible here. FARM, FNETS and GNAR are modelled using a lag of  $L = 1$ . The network  $\mathcal{G} = ([N], \mathcal{E})$  chosen for GNAR is defined by  $(i, j) \in \mathcal{E}$  only if the Euclidean distance between stations  $i$  and  $j$  is less than 3 kilometres.

There were  $K = 7$  clusters estimated by NIRVAR. Figure 7(a) shows the geographic locations of the stations in clusters 3 and 5. Cluster 5 is concentrated around central London whereas the stations in cluster 3 are located further from the center near parks and more residential areas. In contrast to the epsilon ball construction of the GNAR network, the NIRVAR clusters do not necessarily lie within some ball of a given radius. Figure 7(b) shows the mean number of bicycle rides across each of the 7 NIRVAR clusters for every day of the week. The clusters are differentiated by their mean number of bicycle rides as well as by the change in the number of bicycle rides on weekdays compared with weekends. For example, stations in clusters 2 and 5, which are located mainly in central London, have high usage during the week and lower usage during the weekend. This likely corresponds to usage by commuters. In contrast, the usage of bicycles from stations in cluster 3 increases during weekends. This may correspond to usage for leisure by tourists or local residents, considering that many of the stations in this group are

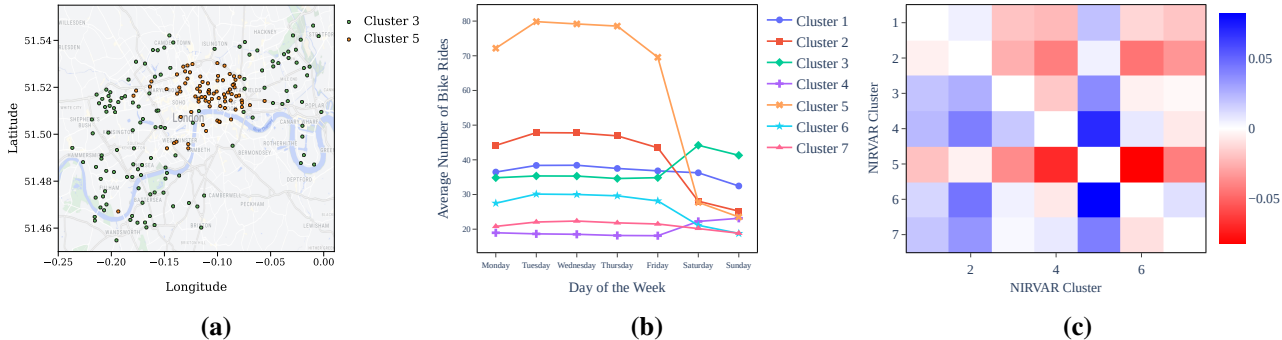


**Figure 7:** NIRVAR on the Santander Cycles dataset. (a) Clusters 3 and 5. (b) Average number of bicycle rides across each of the  $K = 7$  clusters for weekday. (c) Flow between clusters, where each block indicates a net flow from cluster  $i$  into cluster  $j$ .

located around parks.

To analyse the flow of bicycle rides between NIRVAR clusters, we computed a  $K \times K$  matrix  $F$ , where  $F_{ij}$  is the number of bicycle rides that start from any station in cluster  $i$  and end in any station in cluster  $j$ . A matrix  $\tilde{F}$  with elements  $\tilde{F}_{ij} = (F_{ij} - F_{ji}) / (F_{ij} + F_{ji})$ , provides a normalised measure of the imbalance in the flow of bicycle rides between clusters. Figure 7(c) shows  $\tilde{F}_{ij}$ : rows 2 and 5 of  $\tilde{F}$  are negative (red) which corresponds to a net inflow into NIRVAR clusters 2 and 5, whose stations are located mainly in central London.

To conclude, one-day-ahead predictions from NIRVAR, FARM, FNETS and GNAR are obtained using a rolling window backtesting framework from 09/02/2020 until 10/03/2020 (30 days). The overall MSE is homogeneous across models with NIRVAR achieving the lowest value (0.364), followed by FARM (0.370), GNAR (0.374) and FNETS (0.388).

## 7 Discussion

We introduce NIRVAR, a framework for modelling a panel of multivariate time series as a network VAR process. Two key features characterise NIRVAR: first, the underlying network is unobserved; second, the network is reconstructed prior to estimation of the VAR model parameters. This circumvents the need to specify tuning or thresholding hyperparameters when constructing the network, and it avoids estimation of the full, dense VAR parameter matrix. Due to the regularisation induced by the network, NIRVAR is computationally fast. For example, backtesting NIRVAR on the Santander experiment in Section 6.3 for a single forecast took approximately 10 seconds compared with 70 seconds for a VAR<sup>2</sup>.

A drawback of the estimation method is that it will be biased whenever there are edges between blocks of the data generating SBM. Therefore, it is only suitable for assortative graphs. One possible solution to this is to consider a mixed membership SBM (Airoidi et al., 2008) in which each graph vertex can be associated with multiple clusters. We leave this for future research. The NIRVAR model assumes the observed random graph does not change over time. Extending the model to incorporate a time varying adjacency matrix could add flexibility and improve both the cluster assignment and the predictive performance. Another future direction is to extend the methodology to a VAR( $p$ ) by writing it as a VAR(1) in companion matrix form (see Lütkepohl, 2005).

It would be a natural extension to incorporate a factor model into the NIRVAR framework, isolating the idiosyncratic interactions that are due to network effects from the co-movements that are due to common factors. For example, in the financial application, we removed the market factor prior to NIRVAR estimation. Incorporating a factor model would also likely improve the forecasting performance on the FRED-MD dataset. McCracken and Ng (2016) find eight factors in the sample they consider; removing these factors could give prominence to network effects, improving NIRVAR estimation and prediction.

<sup>2</sup>Both experiments were run using a single Intel Core i5-1145G7 CPU.

## Acknowledgements

Brendan Martin acknowledges funding from the Engineering and Physical Sciences Research Council (EPSRC), grant number EP/S023151/1. Francesco Sanna Passino acknowledges funding from the EPSRC, grant number EP/Y002113/1.

## Data availability

All data and *Python* code are available in the GitHub repository [bmartin9/NIRVAR](https://github.com/bmartin9/NIRVAR).

## References

- Ahelegbey, D. F., Billio, M., and Casarin, R. (2016) Bayesian graphical models for structural vector autoregressive processes. *Journal of Applied Econometrics*, **31**, 357–386.
- Airoldi, E. M., Blei, D., Fienberg, S., and Xing, E. (2008) Mixed membership stochastic blockmodels. *Advances in Neural Information Processing Systems*, **21**.
- Athreya, A., Fishkind, D. E., Tang, M., et al. (2017) Statistical inference on random dot product graphs: a survey. *The Journal of Machine Learning Research*, **18**, 8393–8484.
- Bai, J. (2003) Inferential theory for factor models of large dimensions. *Econometrica*, **71**, 135–171.
- Bai, Z. and Silverstein, J. W. (2010) *Spectral analysis of large dimensional random matrices*, vol. 20. Springer.
- Barigozzi, M., Cavaliere, G., and and, G. M. (2025) Factor network autoregressions. *Journal of Business & Economic Statistics*, **0**, 1–28.
- Barigozzi, M., Cho, H., and Owens, D. (2023) FNETS: Factor-adjusted network estimation and forecasting for high-dimensional time series. *Journal of Business & Economic Statistics*, 1–13.
- Chang, J., He, J., Yang, L., and Yao, Q. (2023) Modelling matrix time series via a tensor cp-decomposition. *Journal of the Royal Statistical Society (Series B)*, **85**, 127–148.
- Chen, E. Y., Fan, J., and Zhu, X. (2023) Community network auto-regression for high-dimensional time series. *Journal of Econometrics*, **235**, 1239–1256.
- Chen, Y., Chi, Y., Fan, J., Ma, C., et al. (2021) Spectral methods for data science: A statistical perspective. *Foundations and Trends® in Machine Learning*, **14**, 566–806.
- Dahlhaus, R. (2000) Graphical interaction models for multivariate time series. *Metrika*, **51**, 157–172.
- De Domenico, M., Solé-Ribalta, A., Cozzo, E., et al. (2013) Mathematical formulation of multilayer networks. *Physical Review X*, **3**, 041022.
- Donoho, D., Gavish, M., and Romanov, E. (2023) Screenot: Exact mse-optimal singular value thresholding in correlated noise. *The Annals of Statistics*, **51**, 122–148.
- Efron, B., Hastie, T., Johnstone, I., and Tibshirani, R. (2004) Least angle regression. *The Annals of Statistics*, **32**, 407–451.
- Eichler, M. (2007) Granger causality and path diagrams for multivariate time series. *Journal of Econometrics*, **137**, 334–353.
- Fan, J. and Li, R. (2001) Variable selection via nonconcave penalized likelihood and its oracle properties. *Journal of the American Statistical Association*, **96**, 1348–1360.

- Fan, J., Liao, Y., and Mincheva, M. (2013) Large covariance estimation by thresholding principal orthogonal complements. *Journal of the Royal Statistical Society (Series B)*, **75**, 603–680.
- Fan, J., Masini, R. P., and Medeiros, M. C. (2023) Bridging factor and sparse models. *The Annals of Statistics*, **51**, 1692–1717.
- Gallagher, I., Jones, A., Bertiger, A., Priebe, C. E., and Rubin-Delanchy, P. (2023) Spectral embedding of weighted graphs. *Journal of the American Statistical Association*, 1–10.
- Gallagher, I., Jones, A., and Rubin-Delanchy, P. (2021) Spectral embedding for dynamic networks with stability guarantees. *Advances in Neural Information Processing Systems*, **34**, 10158–10170.
- Gu, S., Kelly, B., and Xiu, D. (2020) Empirical asset pricing via machine learning. *The Review of Financial Studies*, **33**, 2223–2273.
- Guðmundsson, G. S. and Brownlees, C. (2021) Detecting groups in large vector autoregressions. *Journal of Econometrics*, **225**, 2–26.
- Holland, P. W., Laskey, K. B., and Leinhardt, S. (1983) Stochastic blockmodels: First steps. *Social Networks*, **5**, 109–137.
- Hubert, L. and Arabie, P. (1985) Comparing partitions. *Journal of Classification*, **2**, 193–218.
- Jones, A. and Rubin-Delanchy, P. (2020) The multilayer random dot product graph. *arXiv preprint arXiv:2007.10455*.
- Knight, M., Leeming, K., Nason, G., and Nunes, M. (2020) Generalized network autoregressive processes and the GNAR package. *Journal of Statistical Software*, **96**, 1–36.
- Knight, M. I., Nunes, M., and Nason, G. (2016) Modelling, detrending and decorrelation of network time series. *arXiv preprint arXiv:1603.03221*.
- Korkmaz, S., Gökşülük, D., and Zararsiz, G. (2014) MVN: An R package for assessing multivariate normality. *R Journal*, **6**.
- Laloux, L., Cizeau, P., Potters, M., and Bouchaud, J.-P. (2000) Random matrix theory and financial correlations. *International Journal of Theoretical and Applied Finance*, **3**, 391–397.
- Lancichinetti, A. and Fortunato, S. (2009) Community detection algorithms: a comparative analysis. *Physical Review E*, **80**, 056117.
- Lee, C. and Wilkinson, D. J. (2019) A review of stochastic block models and extensions for graph clustering. *Applied Network Science*, **4**, 1–50.
- Lütkepohl, H. (2005) *New introduction to multiple time series analysis*. Springer Science & Business Media.
- Marčenko, V. A. and Pastur, L. A. (1967) Distribution of eigenvalues for some sets of random matrices. *Matematicheskii Sbornik*, **114**, 507–536.
- McCracken, M. W. and Ng, S. (2016) FRED-MD: A monthly database for macroeconomic research. *Journal of Business & Economic Statistics*, **34**, 574–589.
- Nicholson, W. B., Wilms, I., Bien, J., and Matteson, D. S. (2020) High dimensional forecasting via interpretable vector autoregression. *Journal of Machine Learning Research*, **21**, 1–52.
- Rubin-Delanchy, P., Cape, J., Tang, M., and Priebe, C. E. (2022) A statistical interpretation of spectral embedding: The generalised random dot product graph. *Journal of the Royal Statistical Society (Series B)*, **84**, 1446–1473.

- Schönemann, P. H. (1966) A generalized solution of the orthogonal procrustes problem. *Psychometrika*, **31**, 1–10.
- Stock, J. H. and Watson, M. W. (2002) Forecasting using principal components from a large number of predictors. *Journal of the American Statistical Association*, **97**, 1167–1179.
- Tibshirani, R. (1996) Regression shrinkage and selection via the lasso. *Journal of the Royal Statistical Society (Series B)*, **58**, 267–288.
- Vuletić, M., Prenzel, F., and Cucuringu, M. (2024) Fin-GAN: forecasting and classifying financial time series via generative adversarial networks. *Quantitative Finance*, 1–25.
- Whiteley, N., Gray, A., and Rubin-Delanchy, P. (2022) Statistical exploration of the manifold hypothesis. *arXiv preprint arXiv:2208.11665*.
- Zhang, M. and Chen, Y. (2018) Link prediction based on graph neural networks. *Advances in neural information processing systems*, **31**.
- Zhu, M. and Ghodsi, A. (2006) Automatic dimensionality selection from the scree plot via the use of profile likelihood. *Computational Statistics & Data Analysis*, **51**, 918–930.
- Zhu, X., Huang, D., Pan, R., and Wang, H. (2020) Multivariate spatial autoregressive model for large scale social networks. *Journal of Econometrics*, **215**, 591–606.
- Zhu, X., Pan, R., Li, G., Liu, Y., and Wang, H. (2017) Network vector autoregression. *The Annals of Statistics*, **45**, 1096 – 1123.

## SUPPLEMENTARY MATERIAL

### S1 Theory

#### S1.1 Proof of Proposition 3.1

*Proof.* We prove that the covariance matrix  $\Gamma = \mathbb{E}(\mathbf{X}_t \mathbf{X}_t')$  can be written in terms of  $U_\Phi$ . From Lütkepohl (2005), we have that  $\Gamma - \Phi \Gamma \Phi' = \Sigma$ . This is an example of a Lyapunov matrix equation and its formal solution is given by (Young, 1981):

$$\Gamma = \sum_{k=0}^{\infty} (\Phi)^k \Sigma (\Phi')^k,$$

which converges when  $\rho(\Phi) < 1$  (Smith, 1968). Since we assume a stationary NIRVAR process, then indeed  $\rho(\Phi) < 1$  and the series converges. With  $\Sigma = \sigma^2 I_N$  we have

$$\Gamma = \sigma^2 \sum_{k=0}^{\infty} (\Phi)^{2k}. \tag{S.1}$$

Recalling the eigendecomposition

$$\Phi = U_\Phi \Lambda_\Phi U_\Phi' + U_{\Phi,\perp} \Lambda_{\Phi,\perp} U_{\Phi,\perp}', \tag{S.2}$$

we can substitute Equation (S.2) into Equation (S.1),

$$\Gamma = \sigma^2 \sum_{k=0}^{\infty} (U_\Phi \Lambda_\Phi U_\Phi' + U_{\Phi,\perp} \Lambda_{\Phi,\perp} U_{\Phi,\perp}')^{2k} \tag{S.3}$$

$$\begin{aligned}
 &= \sigma^2 \left( U_{\Phi} \sum_{k=0}^{\infty} \Lambda_{\Phi}^{2k} U_{\Phi}' + U_{\Phi, \perp} \sum_{k=0}^{\infty} \Lambda_{\Phi, \perp}^{2k} U_{\Phi, \perp}' \right) \\
 &= \sigma^2 (U_{\Phi} \Lambda_{\Gamma} U_{\Phi}' + U_{\Phi, \perp} \Lambda_{\Gamma, \perp} U_{\Phi, \perp}'),
 \end{aligned}$$

where  $\Lambda_{\Gamma}$  is a diagonal matrix whose diagonal entries are  $(\lambda_{\Gamma})_i = 1/(1 - (\lambda_{\Phi})_i^2)$  with  $(\lambda_{\Phi})_i$  being the  $i$ -th diagonal entry of  $\Lambda_{\Phi}$ . Therefore, the rank  $d$  eigendecomposition of  $\Gamma$  is  $\Gamma = U_{\Phi} \Lambda_{\Gamma} U_{\Phi}'$ .  $\square$

**Remark 3.** Note that the key step in going from the first to the second line of (S.3) relies on  $U_{\Phi}' U_{\Phi} = I_K$ . If we were to relax the assumption of symmetric  $\Phi$  in Proposition 3.1, then (S.2) would be replaced by the SVD,  $\Phi = U_{\Phi} \Lambda_{\Phi} V_{\Phi}' + U_{\Phi, \perp} \Lambda_{\Phi, \perp} V_{\Phi, \perp}'$ . Since  $U_{\Phi}' V_{\Phi} \neq I_K$ , the infinite sum in (S.3) would no longer have a simple form.

## S1.2 Derivation of the NIRVAR generalised least-squares estimator

The generalised least-squares estimator is obtained by minimising the objective

$$\begin{aligned}
 S\{\gamma(\hat{A})\} &= \mathbf{u}(\hat{A})^{(q)'} (I_T \otimes \Sigma^{-1}) \mathbf{u}(\hat{A})^{(q)} \\
 &= \{\mathbf{y}^{(q)} - (X' \otimes I_N) R(\hat{A}) \gamma(\hat{A})\}' (I_T \otimes \Sigma^{-1}) \{\mathbf{y}^{(q)} - (X' \otimes I_N) R(\hat{A}) \gamma(\hat{A})\} \\
 &= \mathbf{y}^{(q)'} (I_T \otimes \Sigma^{-1}) \mathbf{y}^{(q)} + \gamma(\hat{A})' R(\hat{A})' (X X' \otimes \Sigma^{-1}) R(\hat{A}) \gamma(\hat{A}) - 2\gamma(\hat{A})' R(\hat{A})' (X \otimes \Sigma^{-1}) \mathbf{y}^{(q)}.
 \end{aligned}$$

Hence,

$$\frac{\partial S\{\gamma(\hat{A})\}}{\partial \gamma(\hat{A})} = 2R(\hat{A})' (X X' \otimes \Sigma^{-1}) R(\hat{A}) \gamma(\hat{A}) - 2R(\hat{A})' (X \otimes \Sigma^{-1}) \mathbf{y}^{(q)}.$$

Equating to zero gives the normal equations

$$R(\hat{A})' (X X' \otimes \Sigma^{-1}) R(\hat{A}) \gamma(\hat{A}) = R(\hat{A})' (X \otimes \Sigma^{-1}) \mathbf{y}^{(q)},$$

and, consequently, the generalised least-squared estimator is

$$\hat{\gamma}(\hat{A}) = \{R(\hat{A})' (X X' \otimes \Sigma^{-1}) R(\hat{A})\}^{-1} R(\hat{A})' (X \otimes \Sigma^{-1}) \mathbf{y}^{(q)}. \quad (\text{S.4})$$

The Hessian of  $S\{\gamma(\hat{A})\}$ ,

$$\frac{\partial^2 S\{\gamma(\hat{A})\}}{\partial \gamma(\hat{A}) \partial \gamma(\hat{A})'} = 2R(\hat{A})' (X X' \otimes \Sigma^{-1}) R(\hat{A}),$$

is positive definite which confirms that  $\hat{\gamma}(\hat{A})$  is a minimising vector.

## S1.3 Proof of Proposition 4.1

*Proof.* Substituting  $\mathbf{y}^{(q)} = (X' \otimes I_N) R(A) \gamma(A) + \mathbf{u}^{(q)}$  into Equation (S.4) yields

$$\begin{aligned}
 \hat{\gamma}(\hat{A}) &= \{R(\hat{A})' (X X' \otimes \Sigma^{-1}) R(\hat{A})\}^{-1} R(\hat{A})' (X \otimes \Sigma^{-1}) \{(X' \otimes I_N) R(A) \gamma(A) + \mathbf{u}^{(q)}\} \\
 &= \{R(\hat{A})' (X X' \otimes \Sigma^{-1}) R(\hat{A})\}^{-1} R(\hat{A})' (X X' \otimes \Sigma^{-1}) R(A) \gamma(A) \\
 &\quad + \{R(\hat{A})' (X X' \otimes \Sigma^{-1}) R(\hat{A})\}^{-1} R(\hat{A})' (I_{NQ} \otimes \Sigma^{-1}) \text{vec}(U^{(q)} X').
 \end{aligned}$$

Noting that  $\mathbb{E}\{\text{vec}(U^{(q)} X')\} = \mathbb{E}\{(X \otimes I_N)\} \mathbb{E}\{\mathbf{u}^{(q)}\} = 0$ , we see that the bias of the estimator, given  $\hat{A}$ , is  $\mathbb{E}\{\hat{\beta}(\hat{A}) | \hat{A}\} = R(\hat{A}) C \gamma(A)$ , where

$$C := \{R(\hat{A})' (X X' \otimes \Sigma^{-1}) R(\hat{A})\}^{-1} R(\hat{A})' (X X' \otimes \Sigma^{-1}) R(A).$$

We have that  $\text{colsp}\{R(A)\} \subseteq \text{colsp}\{R(\hat{A})\} \iff R(\hat{A})\gamma(\hat{A}) = R(A)\gamma(A) = \beta$ . This is true if and only if  $\mathbb{E}\{\hat{\beta}(\hat{A})|\hat{A}\} = \mathbb{E}(R(\hat{A})\hat{\gamma}(\hat{A})|\hat{A}) = R(\hat{A})\mathbb{E}[\{R(\hat{A})'(XX' \otimes \Sigma^{-1})R(\hat{A})\}^{-1}R(\hat{A})'(XX' \otimes \Sigma^{-1})R(A)\gamma(A)|\hat{A}]$   
 $= R(\hat{A})\mathbb{E}[\{R(\hat{A})'(XX' \otimes \Sigma^{-1})R(\hat{A})\}^{-1}R(\hat{A})'(XX' \otimes \Sigma^{-1})R(\hat{A})\gamma(\hat{A})|\hat{A}] = R(\hat{A})\gamma(\hat{A}) = \beta$ .  $\square$

### S1.4 Proof of Proposition 4.2

*Proof.* The NIRVAR estimator,

$$\hat{\gamma}(\hat{A}) = \{R(\hat{A})'(XX' \otimes \Sigma^{-1})R(\hat{A})\}^{-1}R(\hat{A})'(XX' \otimes \Sigma^{-1})R(A)\gamma(A) + \{R(\hat{A})'(XX' \otimes \Sigma^{-1})R(\hat{A})\}^{-1}R(\hat{A})'(I_{NQ} \otimes \Sigma^{-1})\text{vec}(U^{(q)}X').$$

can be written as

$$\sqrt{T} \left\{ \hat{\gamma}(\hat{A}) - C\gamma(A) \right\} = \left\{ R(\hat{A})' \left( \frac{XX'}{T} \otimes \Sigma^{-1} \right) R(\hat{A}) \right\}^{-1} R(\hat{A})'(I_{NQ} \otimes \Sigma^{-1}) \frac{1}{\sqrt{T}} \text{vec}(U^{(q)}X'). \quad (\text{S.5})$$

By Lemma 3.1 of Lütkepohl (2005),  $\Gamma$  exists and is nonsingular. Also by Lemma 3.1 of Lütkepohl (2005),

$$\frac{1}{\sqrt{T}} \text{vec}(U^{(q)}X') \xrightarrow{d} \mathcal{N}(0, \Gamma \otimes \Sigma). \quad (\text{S.6})$$

By Equation (S.5),

$$\begin{aligned} \text{plim} \left\{ \hat{\gamma}(\hat{A}) - C\gamma(A) \right\} &= \text{plim} \left[ \left\{ R(\hat{A})' \left( \frac{XX'}{T} \otimes \Sigma^{-1} \right) R(\hat{A}) \right\}^{-1} R(\hat{A})'(I_{NQ} \otimes \Sigma^{-1}) \text{vec} \left( \frac{U^{(q)}X'}{T} \right) \right] \\ &= \text{plim} \left[ \left\{ R(\hat{A})' \left( \frac{XX'}{T} \otimes \Sigma^{-1} \right) R(\hat{A}) \right\}^{-1} R(\hat{A})'(I_{NQ} \otimes \Sigma^{-1}) \right] \text{plim} \left\{ \text{vec} \left( \frac{U^{(q)}X'}{T} \right) \right\}, \end{aligned}$$

where the second line follows from Slutsky's Theorem, and the continuous mapping theorem. But Equation (S.6) implies that

$$\text{plim} \left\{ \text{vec} \left( \frac{UX'}{T} \right) \right\} = 0.$$

Thus  $\text{plim}\{\hat{\gamma}(\hat{A}) - C\gamma(A)\} = 0$  (weak consistency). For convenience, we define

$$\hat{G} := \left\{ R(\hat{A})' \left( \frac{XX'}{T} \otimes \Sigma^{-1} \right) R(\hat{A}) \right\}^{-1} R(\hat{A})'(I_{NQ} \otimes \Sigma^{-1}).$$

Then

$$G := \text{plim}(\hat{G}) = \left\{ R(\hat{A})' (\Gamma \otimes \Sigma^{-1}) R(\hat{A}) \right\}^{-1} R(\hat{A})'(I_{NQ} \otimes \Sigma^{-1}).$$

By Proposition C.15(1) of Lütkepohl (2005), Equation (S.6) implies that

$$\hat{G} \frac{1}{\sqrt{T}} \text{vec}(U^{(q)}X') \xrightarrow{d} \mathcal{N}(0, G(\Gamma \otimes \Sigma)G').$$

Thus,  $\sqrt{T}\{\hat{\gamma}(\hat{A}) - C\gamma(A)\}$  is asymptotically normal with asymptotic variance

$$\begin{aligned}
 G(\Gamma \otimes \Sigma)G' &= \\
 &= \left[ \left\{ R(\hat{A})' (\Gamma \otimes \Sigma^{-1}) R(\hat{A}) \right\}^{-1} R(\hat{A})' (I_{NQ} \otimes \Sigma^{-1}) \right] (\Gamma \otimes \Sigma) \left[ \left\{ R(\hat{A})' (\Gamma \otimes \Sigma^{-1}) R(\hat{A}) \right\}^{-1} R(\hat{A})' (I_{NQ} \otimes \Sigma^{-1}) \right]' \\
 &= \left\{ R(\hat{A})' (\Gamma \otimes \Sigma^{-1}) R(\hat{A}) \right\}^{-1} R(\hat{A})' (I_{NQ} \otimes \Sigma^{-1}) (\Gamma \otimes \Sigma) (I_{NQ} \otimes \Sigma^{-1}) R(\hat{A}) \left\{ R(\hat{A})' (\Gamma \otimes \Sigma^{-1}) R(\hat{A}) \right\}^{-1} \\
 &= \left\{ R(\hat{A})' (\Gamma \otimes \Sigma^{-1}) R(\hat{A}) \right\}^{-1} \left\{ R(\hat{A})' (\Gamma \otimes \Sigma^{-1}) R(\hat{A}) \right\} \left\{ R(\hat{A})' (\Gamma \otimes \Sigma^{-1}) R(\hat{A}) \right\}^{-1} \\
 &= \left\{ R(\hat{A})' (\Gamma \otimes \Sigma^{-1}) R(\hat{A}) \right\}^{-1}.
 \end{aligned}$$

□

### S1.5 Proof of Proposition 4.3

*Proof.* By Proposition C.15(1) and Proposition 5.1 of [Lütkepohl \(2005\)](#),

$$\text{var} \left\{ \sqrt{T} \left( \hat{\beta}(A) - \beta \right) \right\} = R(A) \left[ R(A)' \left\{ \Gamma \otimes \Sigma^{-1} \right\} R(A) \right]^{-1} R(A)'. \quad (\text{S.7})$$

By Proposition C.15(1) of [Lütkepohl \(2005\)](#) and Proposition 4.2 of this paper,

$$\text{var} \left( \sqrt{T} \left( \hat{\beta}(\hat{A}) - \beta \right) \right) = R(\hat{A}) \left\{ R(\hat{A})' (\Gamma \otimes \Sigma^{-1}) R(\hat{A}) \right\}^{-1} R(\hat{A})'. \quad (\text{S.8})$$

By Lemma 3.1 of [Lütkepohl \(2005\)](#),  $\Gamma$  is positive definite. By assumption,  $\Sigma$  is positive definite. Given this and the fact that both  $\Gamma$  and  $\Sigma$  are symmetric,  $\Gamma \otimes \Sigma^{-1}$  is positive definite and symmetric. By Observation 7.1.8 of [Horn and Johnson \(2012\)](#), since  $\text{rk}(R(A)) = M$ , then  $R(A)' \left\{ \Gamma \otimes \Sigma^{-1} \right\} R(A)$  is positive definite with rank  $M$ . By inspection,  $R(A)' \left\{ \Gamma \otimes \Sigma^{-1} \right\} R(A)$  is symmetric which implies  $\left[ R(A)' \left\{ \Gamma \otimes \Sigma^{-1} \right\} R(A) \right]^{-1}$  is symmetric and of rank  $M$ . Using Observation 7.1.8 of [Horn and Johnson \(2012\)](#) again, the matrix  $R(A) \left[ R(A)' \left\{ \Gamma \otimes \Sigma^{-1} \right\} R(A) \right]^{-1} R(A)'$  is positive definite with rank  $M$ . By the same argument, the matrix  $R(\hat{A}) \left\{ R(\hat{A})' (\Gamma \otimes \Sigma^{-1}) R(\hat{A}) \right\}^{-1} R(\hat{A})'$  is positive definite with rank  $\widehat{M}$ . The assumption that  $\text{colsp}\{R(A)\} \subseteq \text{colsp}\{R(\hat{A})\}$  implies that

$$\text{colsp} \left[ R(A) \left\{ R(A)' (\Gamma \otimes \Sigma^{-1}) R(A) \right\}^{-1} R(A)' \right] \subseteq \text{colsp} \left[ R(\hat{A}) \left\{ R(\hat{A})' (\Gamma \otimes \Sigma^{-1}) R(\hat{A}) \right\}^{-1} R(\hat{A})' \right].$$

Thus

$$P := R(\hat{A}) \left\{ R(\hat{A})' (\Gamma \otimes \Sigma^{-1}) R(\hat{A}) \right\}^{-1} R(\hat{A})' - R(A) \left\{ R(A)' (\Gamma \otimes \Sigma^{-1}) R(A) \right\}^{-1} R(A)'$$

has  $\widehat{M} - M$  nonzero eigenvalues with all other eigenvalues being 0. Hence,  $P$  is positive semi-definite and

$$\text{var} \left[ \sqrt{T} \left\{ \hat{\beta}(\hat{A}) - \beta \right\} \right] - \text{var} \left[ \sqrt{T} \left\{ \hat{\beta}(A) - \beta \right\} \right] \succeq 0. \quad \square$$

### S1.6 Derivation of the Inverse Marčenko-Pastur Distribution

Suppose  $X \sim f_{\text{MP}}(\eta, \sigma^2)$  where

$$f_{\text{MP}}(x; \eta, \sigma^2) = \begin{cases} \frac{1}{2\pi\sigma^2\eta} \sqrt{(x - x_-)(x_+ - x)} & \text{if } x_- \leq x \leq x_+, \\ 0 & \text{otherwise,} \end{cases}$$

is the Marčenko-Pastur distribution with  $N/T \rightarrow \eta \in (0, 1)$  as  $N, T \rightarrow \infty$ ,  $\sigma^2$  being the variance, and

$$x_{\pm} = \sigma^2(1 \pm \sqrt{\eta})^2$$

being the upper and lower bounds of the support of the distribution.

Let  $Y = 1/X$ . Then the distribution,  $f_{\text{IMP}}$ , of  $Y$ , called the inverse Marčenko-Pastur distribution, has finite support over which its density is

$$\begin{aligned} f_{\text{IMP}}(y; \eta, \sigma^2) &= f_{\text{MP}}(y^{-1}; \eta, \sigma^2) \frac{1}{y^2} = \frac{1}{2\pi\sigma^2\eta y^{-1}} \sqrt{(y^{-1} - x_-)(x_+ - y^{-1})} \frac{1}{y^2} \\ &= \frac{1}{2\pi\sigma^2\eta y^2} \sqrt{[1 - y\sigma^2(1 - \sqrt{\eta})^2][y\sigma^2(1 + \sqrt{\eta})^2 - 1]} \\ &= \frac{1}{2\pi\sigma^2\eta y^2} \sqrt{\sigma^4(1 - \eta)^2 \left( \frac{1}{\sigma^2} \left[ \frac{1 + \sqrt{\eta}}{1 - \eta} \right]^2 - y \right) \left( y - \frac{1}{\sigma^2} \left[ \frac{1 - \sqrt{\eta}}{1 - \eta} \right]^2 \right)} \\ &= \frac{1 - \eta}{2\pi\eta y^2} \sqrt{(y_+ - y)(y - y_-)}, \end{aligned}$$

where

$$y_{\pm} = \frac{1}{\sigma^2} \left( \frac{1 \pm \sqrt{\eta}}{1 - \eta} \right)^2.$$

Therefore, the distribution of  $Y$  is

$$f_{\text{IMP}}(y; \eta, \sigma^2) = \begin{cases} (1 - \eta) \sqrt{(y_+ - y)(y - y_-)} / (2\pi\eta y^2) & \text{if } y_- \leq y \leq y_+, \\ 0 & \text{otherwise.} \end{cases}$$

## S2 Simulation study

### S2.1 Large sample distribution of the NIRVAR estimator

This section reports further results relating to Proposition 4.3 and briefly discussed at the end of Section 5.3. Using the same simulation setting as in Section 5.3, we computed  $\alpha_V$  for different levels of intra-block sparsity of the ground truth network. Figure S.1(a) shows that the ratio  $\alpha_V$  of the asymptotic variance of a NIRVAR estimator to that of an estimator which uses all restrictions grows at a super-linear rate. This rate increases with the number of panel components,  $N$ . We also conducted the same experiment using the FRED-MD dataset from Section 6.2. In this case, it was necessary to estimate the asymptotic variances in Equation (S.7) and Equation (S.8) using the sample covariance matrix  $\mathcal{X}\mathcal{X}'/T$ . Figure S.1(b) shows that in this setting of real data,  $\alpha_V$  grows much faster with increased intra-block sparsity compared with the simulation setting.

### S2.2 Stability properties of UASE on the sample covariance matrix

We simulate data from a NIRVAR model with  $Q = 2$ ,  $N = 400$ ,  $T = 20,000$ ,  $K = 4$ ,  $\rho(\Xi) = 0.9$ , and  $\tilde{\Phi} \propto I_{KN}$ . We set  $A_1^{(1)}, A_1^{(2)} \sim \text{Bernoulli}(B_1)$  and  $A_2^{(1)}, A_2^{(2)} \sim \text{Bernoulli}(B_2)$  where

$$B_1 = \begin{pmatrix} 0.8 & 0.8 & 0.05 & 0.05 \\ 0.8 & 0.8 & 0.05 & 0.05 \\ 0.05 & 0.05 & 0.8 & 0.8 \\ 0.05 & 0.05 & 0.8 & 0.8 \end{pmatrix} \quad B_2 = \begin{pmatrix} 0.8 & 0.8 & 0.05 & 0.05 \\ 0.8 & 0.8 & 0.05 & 0.05 \\ 0.8 & 0.05 & 0.05 & 0.01 \\ 0 & 0 & 0.01 & 0.05 \end{pmatrix}.$$

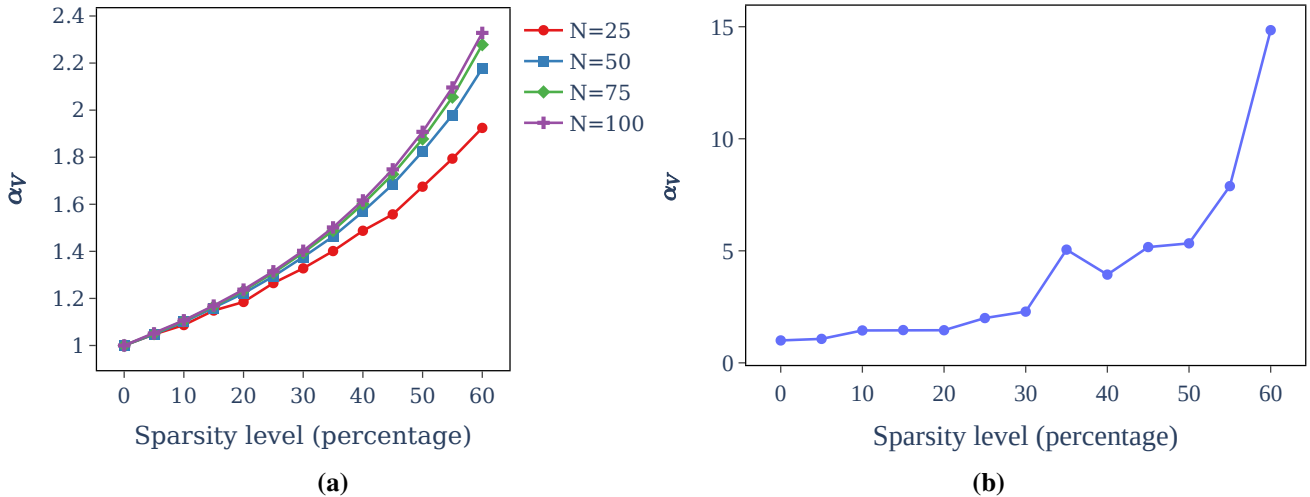


**Figure S.1:** Study of asymptotic variance. (a) Comparing the asymptotic variances of a NIRVAR estimator and an estimator which imposes restrictions within the blocks of the VAR coefficient matrix for different levels of intra-block sparsity and different values of  $N$ . (b) The same comparison as (a) but using FRED-MD data.

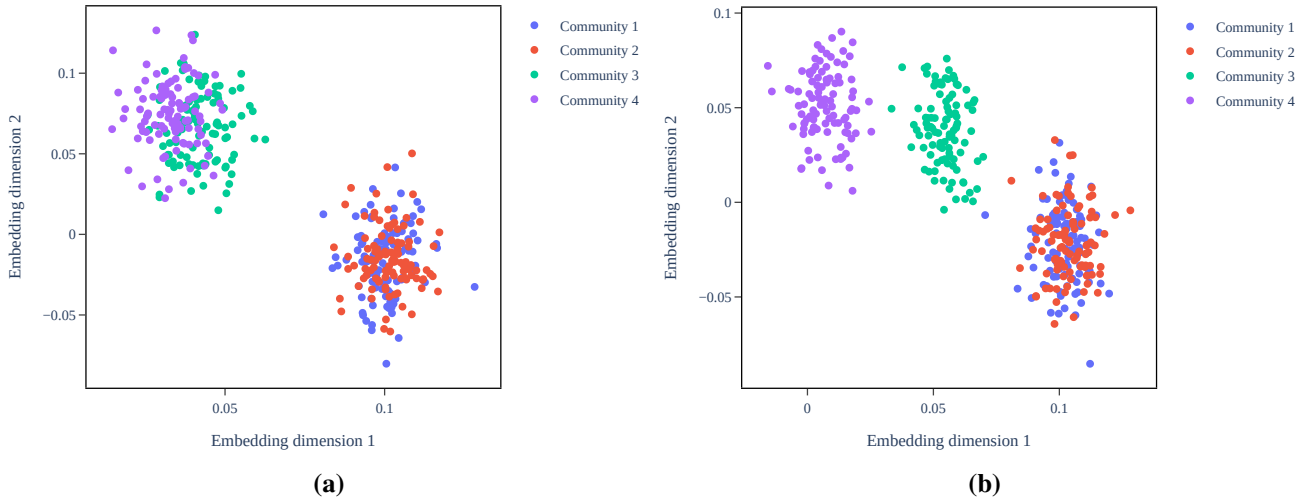


**Figure S.2:** First two dimensions of UASE on the sample covariance matrix for multiple features. (a) Embeddings of feature 1. (b) Embeddings of feature 2.

We will refer to row  $k$  of  $B_1, B_2$  as community  $k$  for  $k = 1, \dots, 4$ . Figure S.2 shows the first two dimensions of the UASE of  $(S^{(1)}|S^{(2)})$  with the embeddings for feature 1 and 2 given by Figure S.2(a) and S.2(b), respectively. Communities 1 and 2 are non-identifiable since the first two rows of  $B_1$  and  $B_2$  are identical. Indeed Figure S.2 shows that the latent positions of vertices in communities 1 and 2 are similar for a given feature and across features, demonstrating both cross-sectional and longitudinal stability. In contrast, row 4 of  $B_1$  is different from row 4 of  $B_2$ , leading to different latent positions for community 4 across features. Moreover, rows 3 and 4 of  $B_2$  are different, leading to a separation of communities 3 and 4 in Figure S.2(b).

### S3 Applications

This section reports some additional results that support the findings discussed in Section 6 of the main document.

### S3.1 FARM, FNETS and GNAR

For convenience, we report the specification of the three models used for benchmarking NIRVAR.

1. **FARM** (Fan et al., 2023). In FARM, the stochastic process  $X_{i,t}$  is modelled as

$$X_{i,t} = \mu_i + \lambda_i \sum_{\ell=1}^L \tau_{\ell} f_{t-\ell} + \sum_{\ell=1}^L \sum_{j=1}^N (\Delta_{\ell})_{ij} \xi_{j,t-\ell} + \epsilon_{i,t},$$

where  $\mu_i$  is the sample mean of series  $i$ ,  $f_t$  is the leading factor at time  $t$  with  $\lambda_i$  the corresponding loading on this factor for series  $i$ , and  $\xi_{j,t}$  is the residual value of series  $i$  after subtracting the contribution of the factor. The parameters  $\tau_{\ell}$  and  $\Delta_{\ell}$  are AR and VAR coefficients for the static factor model and idiosyncratic component, respectively. The factors and loadings are estimated using PCA,  $\tau_{\ell}$  is estimated via OLS, and  $\Delta_{j,\ell}$  is estimated using LASSO, with a penalty parameter selected via BIC.

2. **FNETS** (Barigozzi et al., 2023). In FNETS, the stochastic process  $\mathbf{X}_t$  is modelled as a sum of two latent components: a factor-driven common component  $\boldsymbol{\chi}_t$ , modelled as a generalised dynamic factor model (Forni et al., 2000), and an idiosyncratic component  $\boldsymbol{\xi}_t$ , modelled as a VAR process. This results in the model

$$\mathbf{X}_t = \boldsymbol{\chi}_t + \boldsymbol{\xi}_t, \quad \boldsymbol{\chi}_t = \sum_{\ell=1}^{\infty} \mathbf{\Lambda}_{\ell} \mathbf{f}_{t-\ell}, \quad \boldsymbol{\xi}_t = \sum_{\ell=1}^L \mathbf{\Delta}_{\ell} \boldsymbol{\xi}_{t-\ell} + \mathbf{\Gamma}^{1/2} \boldsymbol{\epsilon}_t,$$

where  $\mathbb{E}(\boldsymbol{\epsilon}_t) = 0$  and  $\text{cov}(\boldsymbol{\epsilon}_t) = I_N$ . Estimation of  $\boldsymbol{\chi}_t$  proceeds by dynamic PCA, whilst for  $\boldsymbol{\xi}_t$ , Barigozzi et al. (2023) propose a  $\ell_1$ -regularised Yule-Walker estimator that requires second-order moments only.

3. **GNAR** (Knight et al., 2020). In GNAR, a simplified model for  $X_{i,t}$  takes the form

$$X_{i,t} = \sum_{\ell=1}^L \left( \alpha_{i,\ell} X_{i,t-\ell} + \beta_{\ell} \sum_{j \in \mathcal{N}(i)} X_{j,t-\ell} \right) + \epsilon_{i,t}, \quad (\text{S.9})$$

where  $\mathcal{N}(i)$  denotes the set of vertices that are connected to vertex  $i$  of a known graph and  $\mathbb{E}(\epsilon_{i,t}) = 0$  with  $\text{var}(\epsilon_{i,t}) = \sigma_i^2$ . The full GNAR model in Knight et al. (2020) extends Equation (S.9) allowing for a time varying known network, edge weights, multiple edge covariates, and stage-neighbours. A key difference between NIRVAR and GNAR is that GNAR assumes the network structure to be known, which is typically not the case in most real-world applications.

### S3.2 Excess market returns

Tables S.1 and S.2 report some additional results supporting the findings discussed in section 6.1 of the main document. We first define some of the statistics used in Table S.1. Letting  $\text{PnL}_t^- := \{\text{PnL}_t : \text{PnL}_t < 0\}$  and  $\text{PnL}^- := \{\text{PnL}_t^-\}_{t=1,\dots,T}$ , we define the Sortino ratio as

$$\text{SortR} = \frac{\text{mean}(\text{PnL})}{\text{stdev}(\text{PnL}^-)} \times \sqrt{252}.$$

The maximum drawdown is defined as

$$\text{MaxDrawdown} = \max_{t,s} \left\{ \frac{\text{CPnL}_t - \text{CPnL}_s}{\text{CPnL}_t} : t < s \right\},$$

where  $\text{CPnL}_t = \sum_{r=1}^t \text{PnL}_r$ . The hit ratio is the mean daily percentage of correct predictions, whereas the long ratio is the mean daily percentage of long predicted positions. The mean absolute error (MAE) and the root mean

	N C1	N C2	N P1	N P2	FARM	FNETS	GNAR
Sharpe Ratio	2.50	2.34	<b>2.82</b>	<u>2.69</u>	0.22	0.78	0.70
Sortino Ratio	4.57	4.18	<b>4.80</b>	<u>4.63</u>	0.36	1.39	1.13
Maximum Drawdown (%)	111	170	<u>61</u>	<b>48</b>	531	107	257
Hit Ratio (%)	50.6	50.6	<b>50.7</b>	<b>50.7</b>	48.7	50.2	41.5
Long Ratio (%)	<u>50.1</u>	49.8	<u>50.1</u>	<b>50.0</b>	49.0	<u>50.1</u>	40.7
Mean RMSE	0.018	0.019	0.018	0.019	0.018	0.018	0.018
Mean Daily PnL (bpts)	2.68	2.49	<b>3.00</b>	<u>2.79</u>	0.44	0.89	1.10
Mean Absolute Error	0.012	0.013	0.012	0.013	0.012	0.012	0.012

**Table S.1:** Statistics on the financial returns predictive performance of each model over the backtesting period. Note that “N” is an abbreviation of NIRVAR. The best performing model is shown in bold, whilst the second best performing model is underlined.

	N C1	N C2	N P1	N P2	FARM	FNETS	GNAR
01/01/2004 - 31/05/2007	4.44	3.09	<b>5.14</b>	<u>4.49</u>	0.56	1.17	1.11
01/06/2007 - 21/10/2010	3.87	4.28	<b>5.08</b>	<u>4.60</u>	0.02	2.05	1.14
22/10/2010 - 19/03/2014	1.91	1.41	<b>3.10</b>	<u>2.36</u>	-0.56	0.46	-0.22
20/03/2014 - 09/08/2017	1.78	<u>2.04</u>	1.41	<b>2.38</b>	-0.37	-0.28	-0.06
10/08/2017 - 31/12/2020	<b>1.70</b>	1.34	<u>1.37</u>	<u>1.37</u>	1.10	0.45	1.07

**Table S.2:** Annualised Sharpe ratios over five equally periods. The best performing model is shown in bold, whilst the second best performing model is underlined.

squared error (MSE) are defined as

$$\text{MAE} = \frac{1}{TN} \sum_{t=1}^T \sum_{i=1}^N \left| \hat{s}_i^{(t)} - s_i^{(t)} \right|, \quad \text{RMSE} = \sqrt{\frac{1}{TN} \sum_{t=1}^T \sum_{i=1}^N \left( \hat{s}_i^{(t)} - s_i^{(t)} \right)^2}.$$

NIRVAR using the precision matrix embedding with or without an additional feature turn out to give the best results across models and indicators.

Table S.2 provides the Sharpe ratio of each model on five equally-spaced intervals of the backtesting period. NIRVAR performs particularly well around the time of the global financial crisis. We also note that NIRVAR P2 and NIRVAR C2 are the best performing models in the fourth sub-period considered, suggesting that the extra feature is beneficial in this period.

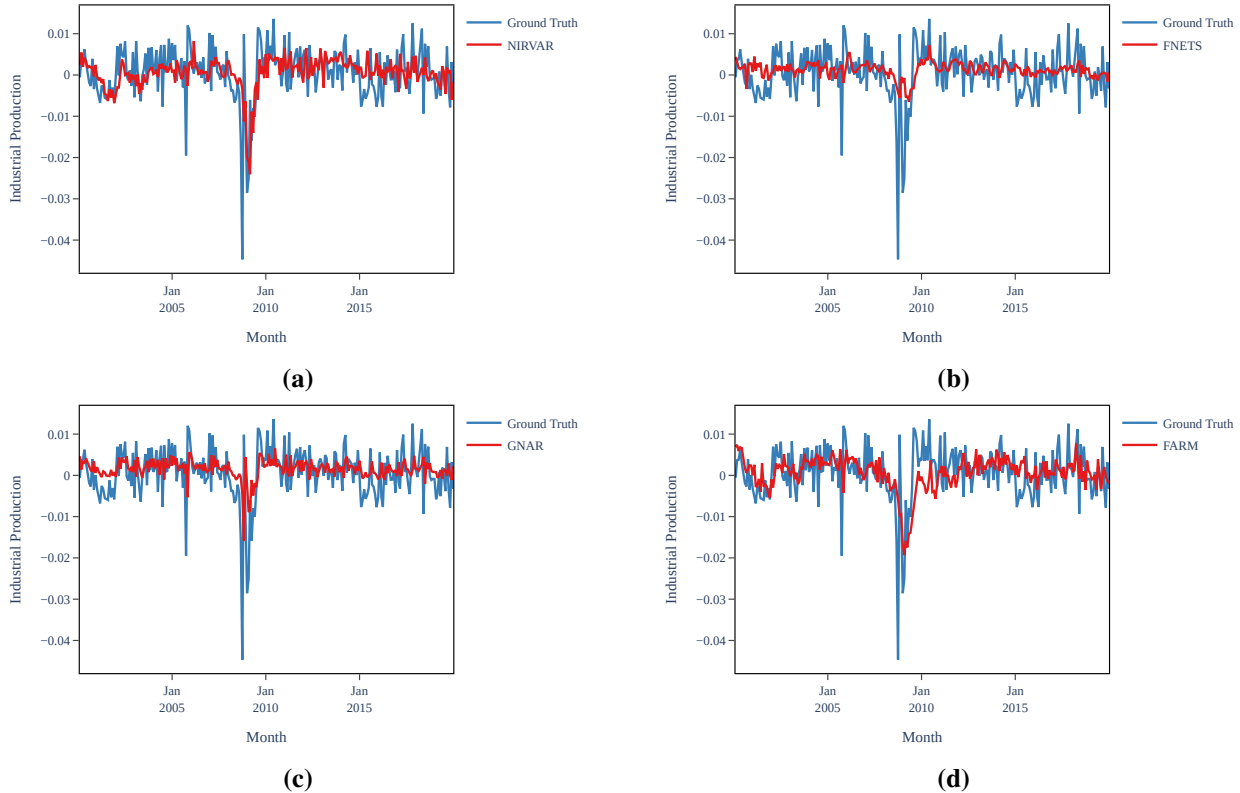
### S3.3 US Industrial production

Table S.3 reports the overall MSE, the sum of the MSE at points for which the model over (under)-estimated the realised value, and the sum of the MSE in extreme and non-extreme regimes where a realised value is defined to be extreme if its magnitude is above the 90-th quantile. NIRVAR, FARM and FNETS give equivalent results, with a slightly better performance of FNETS in non-crisis periods and NIRVAR both overall and in extreme regimes.

Figure S.3 shows the realised difference of the logarithm of IP against the corresponding prediction of each model. Figure S.3(a) and Figure S.3(d) show that both NIRVAR and FARM are more reactive to extreme values than FNETS and GNAR, shown in Figure S.3(b) and Figure S.3(c), respectively.

	NIRVAR	FARM	FNETS	GNAR
Overall MSE	<b>0.0087</b>	<u>0.0089</u>	0.0096	0.0101
MSE: under-estimated	<b>0.0070</b>	<u>0.0076</u>	0.0092	0.0087
MSE: over-estimated	0.0017	<u>0.0013</u>	<b>0.0003</b>	0.0015
MSE: non-extreme	0.0042	0.0042	<b>0.0039</b>	<u>0.0041</u>
MSE: extreme	<b>0.0045</b>	<u>0.0047</u>	0.0057	0.0060

**Table S.3:** Overall MSE and regime statistics for the task of forecasting US IP. The best performing model is shown in bold and the second best performing model is underlined.



**Figure S.3:** Predicted (log-differenced) IP against the realised (log-differenced) IP for each model.

### S3.4 Estimating the scale parameter of the Marčenko-Pastur distribution

The scale parameter of the Marčenko-Pastur distribution is chosen as the value of  $\sigma^2$  that minimises the Kolmogorov-Smirnov statistic:

$$\sigma_*^2 = \arg \min_{\sigma^2} \sup_x |F_{\text{MP}}(x; \eta, \sigma^2) - F_N(x)|, \tag{S.10}$$

where  $F_{\text{MP}}(x; \eta, \sigma^2)$  is the Marčenko-Pastur cumulative distribution and  $F_N(x) = k/N$ , where  $k$  is the number of observations less than or equal to  $x$ , is the observed cumulative step-function of the sample eigenvalues of the covariance matrix. The Marčenko-Pastur cumulative distribution is obtained through numerical integration of  $f_{\text{MP}}(x; \eta, \sigma^2)$ . The minimisation is done using the BFGS algorithm (see, for example, Fletcher, 2000).

One can also consider embedding the correlation matrix instead of the covariance matrix. In this case,  $\sigma^2$  is set equal to 1. As an example, Figure S.4(a) shows a histogram of the eigenvalues of the covariance matrix used in the FRED-MD application in Section 6.2 after the rows and columns of the design matrix were randomly permuted. The best fit Marčenko-Pastur distribution obtained using Equation (S.10) is also plotted in Figure S.4(a) and fits the

histogram well. Figure S.4(b) shows a histogram of the eigenvalues of the correlation matrix corresponding to the FRED-MD application in Section 6.2 after the rows and columns of the design matrix were randomly permuted. The Marčenko-Pastur distribution with  $\sigma^2 = 1$  is also plotted in Figure S.4(b) and fits the histogram well.

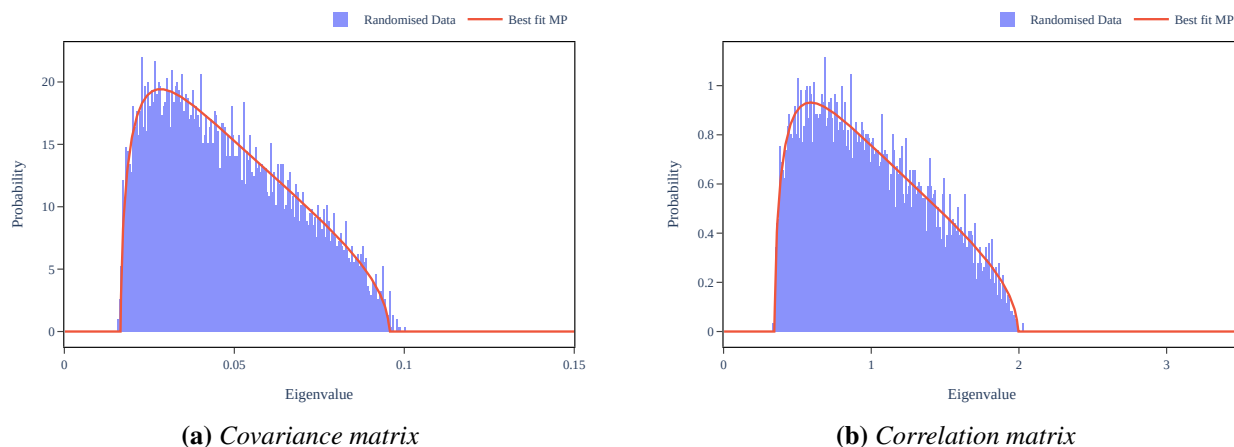


**Figure S.4:** (a) Best fit Marčenko-Pastur distribution alongside the eigenvalues of the covariance matrix used in the FRED-MD application after the rows and columns of the design matrix were randomly permuted. (b) The Marčenko-Pastur distribution with  $\sigma^2 = 1$  alongside the eigenvalues of the correlation matrix used in the FRED-MD application after the rows and columns of the design matrix were randomly permuted.

## Supplementary references

- Barigozzi, M., Cho, H., and Owens, D. (2023) FNETS: Factor-adjusted network estimation and forecasting for high-dimensional time series. *Journal of Business & Economic Statistics*, 1–13.
- Fan, J., Masini, R. P., and Medeiros, M. C. (2023) Bridging factor and sparse models. *The Annals of Statistics*, **51**, 1692–1717.
- Fletcher, R. (2000) *Practical methods of optimization*. John Wiley & Sons.
- Forni, M., Hallin, M., Lippi, M., and Reichlin, L. (2000) The generalized dynamic-factor model: Identification and estimation. *Review of Economics and Statistics*, **82**, 540–554.
- Horn, R. A. and Johnson, C. R. (2012) *Matrix analysis*. Cambridge university press.
- Knight, M., Leeming, K., Nason, G., and Nunes, M. (2020) Generalized network autoregressive processes and the GNAR package. *Journal of Statistical Software*, **96**, 1–36.
- Lütkepohl, H. (2005) *New introduction to multiple time series analysis*. Springer Science & Business Media.
- Smith, R. (1968) Matrix equation  $XA + BX = C$ . *SIAM Journal on Applied Mathematics*, **16**, 198–201.
- Young, N. (1981) The rate of convergence of a matrix power series. *Linear Algebra and its Applications*, **35**, 261–278.